EMBED IN ENSEMBLE TO RIGOROUSLY AND ACCURATELY HOMOGENIZE QUASI-PERIODIC MULTI-SCALE HETEROGENEOUS MATERIAL

ANTHONY ROBERTS [1, †]

Abstract

For microscale heterogeneous partial differential equations (PDEs), this article further develops novel theory and methodology for their macroscale mathematical/asymptotic homogenization. This article specifically encompasses the case of quasi-periodic heterogeneity with finite scale separation: no scale separation limit is required. A key innovation herein is to analyse the ensemble of all phase-shifts of the heterogeneity. Dynamical systems theory then frames the homogenization as a slow manifold of the ensemble. Depending upon any perceived scale separation *within* the quasi-periodic heterogeneity, the homogenization may be done in either one step or two sequential steps: the results are equivalent. The theory not only assures us of the existence and emergence of an exact homogenization at finite scale separation, it also provides a practical systematic method to construct the homogenization to any specified order. For a class of heterogeneities, we show that the macroscale homogenization is potentially valid down to lengths which are just twice that of the microscale heterogeneity! This methodology complements existing well-established results by providing a new rigorous and flexible approach to homogenization that potentially also provides correct macroscale initial and boundary conditions, treatment of forcing and control, and analysis of uncertainty.

[†] This is a contribution to the series of invited papers by past ANZIAM medallists (Editorial, Issue 52(1)). Anthony Roberts was awarded the 2023 ANZIAM medal.

[1]School of Mathematical Sciences, University of Adelaide, Adelaide, South Australia, Australia; e-mail: profajroberts@protonmail.com

1. Introduction

Many engineering and scientific structures have important microscale variations, such as lattice materials [6, 62, 63], the windings in electrical machinery [58], electromagnetism in micro-structured material [20, 44], food drying [70] and slow Stokes flow through porous media [11]. The engineering challenge is to predict and understand the dynamics on a system scale significantly larger than the microscale details. Homogenization, via the recognition of multiple physical length scales, is the common approach [1, 17, 26, 30]. This article further develops an alternative approach to homogenized modelling of the large scale dynamics via a newly established general rigorous theory [52, Section 2.5]. This new complementary approach provides a route to systematic refinements of the homogenization for a *finite* separation of scales and to novel quantification of the remainder error. The significance of this work is not that it effectively reproduces some classic homogenization results, but that it invokes a powerful dynamical systems framework [12, 16, 19, 32, 42, 69] which provides complementary new insights and powerful practical extensions of previously known aspects of homogenization. Consequently, a background in modern dynamical systems [64, 65] is useful to appreciate the direction developed here for homogenization.

Consider materials with complicated microstructure: we want to model their large-scale dynamics by equations with effective 'average' coefficients. Heterogeneous diffusion in one-dimensional (1D) space is the simplest such class of systems: suppose the material, in spatial domain $[0, L]$, has structure so that 'material' or 'heat' $u(t, x)$ diffuses according to

$$\frac{\partial u}{\partial t} = \frac{\partial}{\partial x}\left\{\kappa(x)\frac{\partial u}{\partial x}\right\}, \quad 0 < x < L, \tag{1.1}$$

where the heterogeneous diffusion coefficient $\kappa(x)$ has some complicated multiscale structure. For definiteness, let us initially suppose the macroscale boundary conditions are simply that u is L-periodic in space x (the end of Section 2 discusses other boundary conditions). Our challenge is to derive, support and characterize the macroscale model PDE

$$\frac{\partial U}{\partial t} = K\frac{\partial^2 U}{\partial x^2} + \cdots \tag{1.2}$$

for some effective mean field $U(x, t)$, some effective macroscale diffusivity K, with some higher order corrections, and possibly an error estimate—both the latter represented by the ellipsis "..." in (1.2). The problem we address is *not* to find approximate solutions to PDE (1.1), but instead to provide new justification, construction and interpretation of the simpler PDE (1.2), and cognate higher-order PDEs, as purely macroscale models of the multiscale PDE (1.1). I also comment throughout on the closely connected problem [1, 3, 18, 25, 61] of wave propagation through

heterogeneous material,

$$\frac{\partial^2 u}{\partial t^2} = \frac{\partial}{\partial x}\left\{\kappa(x)\frac{\partial u}{\partial x}\right\} \xrightarrow{\text{homogenized}} \frac{\partial^2 U}{\partial t^2} = K\frac{\partial^2 U}{\partial x^2} + \cdots, \tag{1.3}$$

and this corresponding effective homogenized PDE model that predicts its macroscale dispersive waves. The homogenization approach for both classes are much the same, so the results here apply to elastic materials and other waves, with some caveats. However, the treatment and theory is clearer and more rigorous for the class of diffusive systems (1.1).

Here we focus on cases where the heterogeneity $\kappa(x)$ is quasi-periodic in space. For an example application, Sections 4 and 5 focus on homogenization for the family of heterogeneous diffusivities $\kappa = 1/[1 + a_1 \cos(2\pi x/\ell_1) + a_2 \cos(2\pi x/\ell_2)]$ for arbitrary microscale periods ℓ_1, ℓ_2 with $\ell_1 > \ell_2$. Sections 2 and 3 develop theory and supporting characteristics of homogenization in the general case where the heterogeneity κ is expressible as a function of two variables, say $\kappa(x_1, x_2)$, in which κ is ℓ_i-periodic in variable x_i. Then the quasi-periodic heterogeneity in (1.1) is $\kappa(x, x)$. I emphasize that this work does *not* address the PDE $u_t = \partial_x\{\kappa(x/\epsilon, x/\epsilon)u_x\}$: there is *no* ϵ in the analysis here; and consequently, and in contrast to extant well established theory of quasi-periodic homogenization (for example, see [33], [2, Section 7.4]), the framework here does *not* invoke the infinite length scale separation limit "$\epsilon \to 0$". Instead, the results herein apply for *finite* scale separation (quantified by Section 5), and form arbitrarily high-order homogenizations, not just leading order [33] nor just second-order [57].

Clearly, the approach developed here straightforwardly extends to an arbitrary number of incommensurable periods in the structure of the diffusivity κ, but for simplicity of introducing the key new ideas, techniques and results, we address here the case of just two periods in κ.

Most extant conventional approaches to practically computing a homogenization depend upon the identification of a *representative volume element* (RVE) [62], or a representative cell. Even in the simple case of periodic media, an uncertain issue is an appropriate size of an RVE [34, 38, 43, 59, 60, 63, p. 2, Section 5.1, Section 2.3, Section 1.2.2, p. 2, p. 13, respectively]. A further issue with such RVE-based arguments is that for quasi-periodic heterogeneities, there is *no* one RVE [5, Section 2.1]. When the ratio between microscale lengths ℓ_1, ℓ_2 is irrational, then all volume elements, no matter what size is chosen, are different: no volume element is representative. Relatedly, when the microscale lengths ℓ_1, ℓ_2 have a large least common multiple, then any true RVE must be correspondingly large—resulting in onerous analysis or computation. For example, Blanc and Le Bris [9] comment that for quasi-periodic homogenization, "cell problems must be in general set on the whole space": herein, we show that this "must" is incorrect for our approach. In contrast to "the whole space", here, Sections 2 and 3 instead develop a novel rigorous systematic approach that uses an 'RVE' cell which is the size of the largest microscale length, $\max\{\ell_1, \ell_2\}$, albeit an RVE of more 'spatial' dimensions.

I expect straightforward extensions of the approach developed herein to empower cognate analysis and modelling of the following:

- cases where the heterogeneity is quasi-periodic in any number of microscale lengths $\ell_1 > \ell_2 > \ell_3 > \cdots$;
- PDEs (1.1) where the field u is itself in a vector space such as the cross-sectional structure of either shear dispersion [40, 41], or of elastic beams [49];
- multiple macroscale space dimensions as in the modelling of plates and shells [55];
- PDEs like (1.1) but with macroscale variations in the material parameters as well as microscale variations [5]—sometimes called *functionally graded materials*;
- PDEs like (1.1) but with nonlinear effects [38]—in contrast to the experience of Blanc and Le Bris [9], in the framework developed here, nonlinear problems do not involve any difficulty other than extra algebraic details.

Further, Section 6 shows that the approach, analysis and results developed herein also include three-scale multiscale systems where notionally $\ell_2 \ll \ell_1 \ll L$, that is, where there is a microscale, a mesoscale and a macroscale [21, 45].

Other analytic techniques such as mathematical homogenization or the method of multiple scales [18, 61] provide a mechanism for deriving effective PDE models such as (1.2). However, such previous underlying theory requires the limit of infinite scale separation between the microscale "cell"-sizes ℓ_i and the macroscale domain size L by invoking $\epsilon := \ell_i/L \to 0$ (for example, [2, 6, 70, p. 5, p. 6 and Section 2.4, respectively] and [4]). In contrast, and arising from developments in dynamical systems, Sections 2 and 3 respectively use phase-shift embedding and slowly varying theory [52, 55] to provide rigorous support to the modelling at finite scale separation: that is, when the macroscale length scale L of interest is larger than the microscales ℓ_1 and ℓ_2, but not infinitely so. In the approach here, not only is there no limit, there is no need for such a defined "ϵ". Such finite scale separation empowers this approach to capture the dispersion in wave homogenization which Abdulle and Pouchon [1, p. 3] call for in their discussion stating that "new effective models are required". The phase-shift embedding developed here further illustrates the general principle that macroscale models of microscale structures are often best phrased as ensemble averages [8, 23, 68].

It is well recognized that homogenization is physically effective for reasonably well separated length scales: that the resolved macroscale structures, with length ℓ_M say, satisfy $\ell_M \gg \ell_1$. But what does this mean? Much extant homogenization theory requires the mathematical limit $\ell_1/\ell_M \to 0$. However, *physically*, the ratio ℓ_1/ℓ_M is always finite. By setting homogenization in a new rigorous framework, Section 5 analyses homogenization for finite ℓ_1/ℓ_M to high-order and presents evidence that, in a class of problems, a *quantitative* limit to the spatial resolution of homogenization is that $\ell_1/\ell_M \lesssim 1/2$, equivalently, $\ell_M \gtrsim 2\ell_1$. Mathematically, a wider scale separation is not necessary for homogenization.

Of course, practically, we usually prefer a wider scale separation because of many complicating factors in construction and use of practical homogenization models. However, in the sense discussed by Section 5, this quantitative, near-sharp, lower bound on the required scale separation indicates how little scale separation is necessary. Indeed, because it applies at finite scale separation, the analysis here encompasses *high-contrast media* and so also detects features occurring in this particularly interesting class of problems [17, p. 2].

The new approach to homogenization that we develop here creates a powerful dynamical systems framework for addressing other modelling issues in the future. For a time-dependent simulation of homogenized dynamics, one must provide some initial conditions for the homogenized PDE (1.2). These initial conditions are surprisingly nontrivial at finite scale separation, but the new framework developed here comes with well-established methods to derive the correct initial conditions for long-term forecasts [19, 47, 49, 51]. The projection that provides the correct initial conditions, also provides the correct projection of any applied "forcing" [47, Section 7], including the cases of control and system uncertainty. System uncertainty is a challenge for other techniques [4, 38, p. 3 and Section 8, respectively]. Further, the homogenized PDE (1.2) needs macroscale boundary conditions—a "highly challenging problem" according to Shahraki and Guzina [61], and which Cornaggia and Guzina [18] called a "complex problem that is still an active research topic". Such boundary conditions are nontrivial and it is well recognized that consideration of boundary layers must be accounted for. However, again the new framework developed here comes with a rigorous approach to derive correct boundary conditions for (1.2) to empower accurate predictions at finite scale separation [14–16, 48, 49]. For an example in a different field but cognate to the macroscale modelling developed here, Mercer and Roberts [41] generalized the advection-diffusion 'homogenization' model of shear dispersion in a narrow pipe to arbitrary order and to a quantitative bound on the spatial resolution (its Section 2), with guaranteed accurate initial conditions (its Section 3), and correct macroscale boundary conditions at the pipe's entry and exit (its Section 4). That is, this dynamical systems approach to homogenization potentially provides a rational complete modelling of not just the PDE at finite scale separation, but also material variations, uncertainty, control, forcing, and initial and boundary conditions. In their review of nonlinear homogenization, Matous et al. [38, Section 8] commented that "verification ensures both order of accuracy and consistency . . . and even mathematical foundations for verification are lacking"—the approach developed here provides the required mathematical foundation.

The new approach developed herein has no need of a variational formulation of the governing equations [4, 6, Section 3 and Section 2.4, respectively], and so applies to a much wider class of problems than many extant homogenization methods.

Throughout this article, in the details of the construction of homogenizations, one may observe that the variables x_0, x_1, x_2 appear in much the same sort of algebraic expressions as traditionally obtained by the method of multiple scales. What this parallelism implies is that in suitable circumstances, the algebraic machinations of

the method of multiple scales are indeed sound [52, Corollary 12]. What is new here is that we place such algebraic details in a new, more rigorous and more extensive framework. The new framework developed here improves the clarity, precision, power and physical interpretability of homogenization.

2. Phase-shift embedding

Let us embed the specific given physical quasi-periodic PDE (1.1) into a family of PDE problems formed by all phase-shifts of the quasi-periodic microscale. This embedding is a novel and rigorous twist to the concept of an RVE.

As indicated by Figure 1, we create the desired embedding by considering a field $\mathfrak{u}(t, x_0, x_1, x_2)$ satisfying the PDE

$$\frac{\partial \mathfrak{u}}{\partial t} = \left(\frac{\partial}{\partial x_0} + \frac{\partial}{\partial x_1} + \frac{\partial}{\partial x_2} \right) \left\{ \kappa(x_1, x_2) \left(\frac{\partial \mathfrak{u}}{\partial x_0} + \frac{\partial \mathfrak{u}}{\partial x_1} + \frac{\partial \mathfrak{u}}{\partial x_2} \right) \right\} \tag{2.1}$$

in the domain $\mathcal{D} := \{(x_0, x_1, x_2) \mid x_i \in [0, \ell_i]\}$, for the macroscale $\ell_0 := L$, the specified microscale ℓ_1, ℓ_2 and with ℓ_i-periodic boundary conditions in x_i. We assume $\kappa(x_1, x_2) \geq \kappa_{\min} > 0$. The domain $\mathcal{D}$ in $x_0 x_1 x_2$-space (Figure 1) is often termed *cylindrical* as it is long and thin. I emphasize that this domain has finite aspect ratio: we do *not* take any limit involving its aspect ratio tending to zero nor to infinity.

Figure 1 indicates that we consider $x_0 = x$. The distinction between x_0 and x is that partial derivatives in x_0 are done keeping the other x_i constant, whereas partial derivatives in x are done keeping phases ϕ_i constant.

LEMMA 2.1. *For every solution $\mathfrak{u}(t, x_0, x_1, x_2)$ of the embedding PDE (2.1) and for every vector of phases $\vec{\phi} := (\phi_1, \phi_2)$, the field $u_{\vec{\phi}}(t, x) := \mathfrak{u}(t, x, x + \phi_1, x + \phi_2)$ (that is, the field $\mathfrak{u}$ evaluated on the solid-blue lines in Figure 1) satisfies the heterogeneous diffusion PDE*

$$\frac{\partial u_{\vec{\phi}}}{\partial t} = \frac{\partial}{\partial x} \left\{ \kappa(x + \phi_1, x + \phi_2) \frac{\partial u_{\vec{\phi}}}{\partial x} \right\}. \tag{2.2}$$

Hence, the field $u(t, x) := \mathfrak{u}(t, x, x, x)$ satisfies the given heterogeneous PDE (1.1).

Recall that the most common cell boundary conditions assumed for RVEs are periodic, although in the usual homogenization arguments, other boundary conditions are equally as valid in practice albeit giving slightly different results [39]. In contrast, here the ℓ_1, ℓ_2-periodic cell boundary conditions are *not* assumed, but arise naturally due to the ensemble of phase-shifts. That is, what previously had to be assumed, here arises naturally.
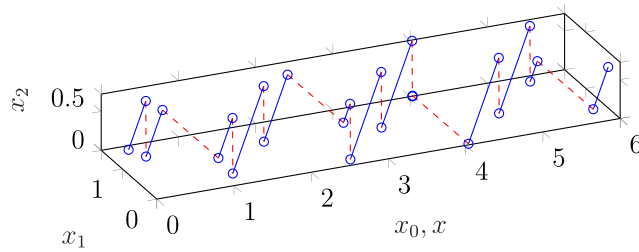
FIGURE 1. Schematic cylindrical domain $\mathcal{D}$ of the multiscale embedding PDE (2.1) for a field $\mathfrak{u}(t, x_0, x_1, x_2)$ (here $L = \ell_0 = 6$, $\ell_1 = 1.62$, $\ell_2 = 0.72$). We obtain solutions of the heterogeneous diffusion PDE (1.1), or (2.2), on such blue lines as $u(t, x) = \mathfrak{u}(t, x, x + \phi_1, x + \phi_2)$ for every pair of constant phases ϕ_1 and ϕ_2 (here $\phi_1 = 0.82$ and $\phi_2 = 0.32$), and where the last two arguments of $\mathfrak{u}$ are modulo ℓ_1 and ℓ_2, respectively.

PROOF. Start by considering the left-hand side time derivative in PDE (2.2):

$$
\begin{aligned}
\frac{\partial u_{\vec{\phi}}}{\partial t} &= \frac{\partial}{\partial t} \mathfrak{u}(t, x, x + \phi_1, x + \phi_2) \\
&= \left[\frac{\partial \mathfrak{u}}{\partial t} \right]_{(t,x,x+\phi_1,x+\phi_2)} \quad \text{(which by PDE (2.1) becomes)} \\
&= \left[\left(\frac{\partial}{\partial x_0} + \frac{\partial}{\partial x_1} + \frac{\partial}{\partial x_2} \right) \left\{ \kappa(x_1, x_2) \left(\frac{\partial \mathfrak{u}}{\partial x_0} + \frac{\partial \mathfrak{u}}{\partial x_1} + \frac{\partial \mathfrak{u}}{\partial x_2} \right) \right\} \right]_{(t,x,x+\phi_1,x+\phi_2)} \\
&= \frac{\partial}{\partial x} \left\{ \left[\kappa(x_1, x_2) \left(\frac{\partial \mathfrak{u}}{\partial x_0} + \frac{\partial \mathfrak{u}}{\partial x_1} + \frac{\partial \mathfrak{u}}{\partial x_2} \right) \right]_{(t,x,x+\phi_1,x+\phi_2)} \right\} \\
&= \frac{\partial}{\partial x} \left\{ \kappa(x + \phi_1, x + \phi_2) \left[\frac{\partial \mathfrak{u}}{\partial x_0} + \frac{\partial \mathfrak{u}}{\partial x_1} + \frac{\partial \mathfrak{u}}{\partial x_2} \right]_{(t,x,x+\phi_1,x+\phi_2)} \right\} \\
&= \frac{\partial}{\partial x} \left\{ \kappa(x + \phi_1, x + \phi_2) \frac{\partial}{\partial x} \mathfrak{u}(t, x, x + \phi_1, x + \phi_2) \right\} \\
&= \frac{\partial}{\partial x} \left\{ \kappa(x + \phi_1, x + \phi_2) \frac{\partial u_{\vec{\phi}}}{\partial x} \right\},
\end{aligned}
$$

namely the right-hand side of (2.2). Hence, provided PDE (2.1) has boundary conditions of ℓ_i-periodicity in x_i, every solution of the embedding PDE (2.1) gives a solution of the original PDE (1.1) for every multi-dimensional phase-shift $\vec{\phi}$ of the heterogeneity.

In particular, the field $u_{\vec{0}}(t, x)$ satisfies the given heterogeneous PDE (1.1). □

LEMMA 2.2 (Converse). *Suppose we have a set of solutions $u_{\vec{\phi}}(t, x)$ of the phase-shifted PDE (2.2)—a set parametrized by the phase vector $\vec{\phi}$—and the set depends smoothly upon $t, x, \vec{\phi}$. Then the field $\mathfrak{u}(t, x, x_1, x_2) := u_{(x_1-x, x_2-x)}(t, x)$ satisfies the embedding PDE (2.1).*

Proof. First, from the PDE (2.1), consider

$$\frac{\partial \mathfrak{u}}{\partial x_0} + \frac{\partial \mathfrak{u}}{\partial x_1} + \frac{\partial \mathfrak{u}}{\partial x_2} = -\frac{\partial u_{\vec{\phi}}}{\partial \phi_1} - \frac{\partial u_{\vec{\phi}}}{\partial \phi_2} + \frac{\partial u_{\vec{\phi}}}{\partial x} + \frac{\partial u_{\vec{\phi}}}{\partial \phi_1} + \frac{\partial u_{\vec{\phi}}}{\partial \phi_2} = \frac{\partial u_{\vec{\phi}}}{\partial x}.$$

Second, since $\phi_i = x_i - x$, that is, $x_i = x + \phi_i$, then

$$\left(\frac{\partial}{\partial x_0} + \frac{\partial}{\partial x_1} + \frac{\partial}{\partial x_2}\right)\kappa(x_1, x_2) = \frac{\partial}{\partial x}\kappa(x + \phi_1, x + \phi_2).$$

Third, hence the right-hand-side of PDE (2.1) becomes

$$\left(\frac{\partial}{\partial x_0} + \frac{\partial}{\partial x_1} + \frac{\partial}{\partial x_2}\right)\left\{\kappa(x_1, x_2)\frac{\partial u_{\vec{\phi}}}{\partial x}\right\}$$

$$= \frac{\partial}{\partial x}\kappa(x + \phi_1, x + \phi_2)\frac{\partial u_{\vec{\phi}}}{\partial x} + \kappa(x_1, x_2)\left(\frac{\partial}{\partial x_0} + \frac{\partial}{\partial x_1} + \frac{\partial}{\partial x_2}\right)\frac{\partial u_{\vec{\phi}}}{\partial x}$$

$$= \frac{\partial}{\partial x}\kappa(x + \phi_1, x + \phi_2)\frac{\partial u_{\vec{\phi}}}{\partial x} + \kappa(x + \phi_1, x + \phi_2)\frac{\partial^2 u_{\vec{\phi}}}{\partial x^2}$$

$$= \frac{\partial}{\partial x}\left\{\kappa(x + \phi_1, x + \phi_2)\frac{\partial u_{\vec{\phi}}}{\partial x}\right\},$$

the right-hand side of PDE (2.2). Lastly, since $\partial \mathfrak{u}/\partial t = \partial u_{\vec{\phi}}/\partial t$, it follows that $\mathfrak{u} := u_{(x_1-x, x_2-x)}(t, x)$ satisfies the embedding PDE (2.1).   □

Corresponding results to Lemmas 2.1 and 2.2 hold for the heterogeneous wave PDE $u_{tt} = \partial_x\{\kappa(x)u_x\}$, with $\partial/\partial t$ replaced by $\partial^2/\partial t^2$.

Consequently, PDEs (2.1) and (2.2) are equivalent, and they may provide us with a set of solutions for an ensemble of materials all with the same microscale heterogeneity structure, but with the structural phase of the material shifted through all possibilities. The key difference between PDEs (2.1) and (2.2) is that although PDE (2.2) is heterogeneous in space x (as is (1.1)), the embedding PDE (2.1) is *homogeneous* in x_0. Because of this homogeneity, Section 3 is empowered to apply an existing rigorous theory for slow variations in space that leads to the desired homogenized model PDE (1.2).

Discussion on translational symmetry. One should look at a macroscale homogenized model such as PDE (1.2) and wonder from where the *continuous x*-translation symmetry comes. The symmetry is not in the underlying microscale heterogeneous PDE (1.1). In the case where heterogeneity $\kappa(x)$ is periodic, the PDE (1.1) has *discrete x*-translational symmetry, which via the infinite scale separation limit as $\ell_1 \to 0$, might be viewed as approximately the continuous symmetry in the homogenization. However, in the case of quasi-periodic heterogeneity $\kappa(x)$, for incommensurate ℓ_1 and ℓ_2, there is *no* discrete translational symmetry. Instead of such a problematic limit, we here instead create the continuous translational symmetry by considering all together the family of problems formed by all phase shifts of the heterogeneity—the PDEs (2.1)

and (2.2). The analysis of the whole family then naturally provides the continuous
x-translational symmetry then inherited by the homogenization (1.2).

How does one get predictions correct for a specific heterogeneity? That is, for a
given specific phase? The answer is that it is the correct boundary conditions for the
homogenization PDE (1.2) that both reflect the specific phase of the heterogeneity at
and near a specific boundary, and that also account for boundary layers. Such boundary
conditions lie just beyond the scope of this article, but should be derivable from those
for the microscale PDE (1.1) by further developing established dynamical systems
analysis [14–16, 41, 48, 49].

3. The slow manifold of any-order homogenization

Let us analyse the embedding PDE (2.1) for a useful slow manifold. This slow
manifold expresses and supports the emergence of a precise homogenization of the
original heterogeneous PDE (1.1). Since the PDEs herein are linear, the slow manifold
is more specifically a slow subspace, but I use the term *manifold* as the same
framework and theory immediately also applies to cognate nonlinear systems.

Rigorous theory [52], inspired by earlier more formal arguments [50, 46], estab-
lishes how to create a PDE model for the macroscale spatial structure of PDE solutions
in cylindrical domains $\mathcal{D}$ like Figure 1. The technique is to base analysis on the case
where variations in x_0 are approximately negligible, and then treat slow, macroscale,
variations in x_0 as a regular perturbation [53, Part III][1].

Being "regular", the perturbation analysis proceeds to any chosen order N in the
'small' derivatives in x_0. For two examples, the usual leading order homogenizations
are the case $N = 2$, and the so-called second-order homogenizations [5, 18, 31]
correspond to the higher-order $N = 4$. Here we consider arbitrary order N. To ensure
the required derivatives and operators exist and have requisite properties, we analyse
the systems in Sobolov spaces $\mathbb{H}_D := W^{N+1,2}(D)$ for various spatial domains D.

To establish the basis of a slow manifold, consider PDE (2.1), in the Sobolov space
with $\mathbb{H}_{\mathcal{D}}$, with $\partial/\partial x_0$ neglected:

$$\frac{\partial u}{\partial t} = \left(\frac{\partial}{\partial x_1} + \frac{\partial}{\partial x_2}\right)\left\{\kappa(x_1, x_2)\left(\frac{\partial u}{\partial x_1} + \frac{\partial u}{\partial x_2}\right)\right\}, \tag{3.1}$$

called the *cell problem*, to be solved with ℓ_i-periodic boundary conditions in x_i. The
basis applies at each and every x_0. Hence, at every x_0, we consider PDE (3.1) on the
Sobolov space $\mathbb{H}_C$, where C is the x_1x_2-cross-section of $\mathcal{D}$.

ASSUMPTION 3.1. Consider the cell eigen-problem for $u \in \mathbb{H}_C$,

$$\lambda u = \left(\frac{\partial}{\partial x_1} + \frac{\partial}{\partial x_2}\right)\left\{\kappa(x_1, x_2)\left(\frac{\partial u}{\partial x_1} + \frac{\partial u}{\partial x_2}\right)\right\},$$

---

[1]Alternatively, in linear problems, one could justify the analysis via a Fourier transform in x_0 [53, 46, Ch. 7 and
Section 2, respectively]. However, for nonlinear problems, it is better to analyse in physical space, so we do so
herein—except for Section 5.

with ℓ_i-periodic boundary conditions in x_i. We assume that $\kappa(x_1, x_2) \geq \kappa_{\min} > 0$ is regular enough that the set of eigenvectors are complete in $\mathbb{H}_C$.

Equilibria. A family of equilibria of (3.1) is $\mathfrak{u}(t, x_1, x_2) = U$, constant in x_1, x_2, for every U. This family, in $\mathbb{H}_C$ for every x_0, forms a subspace of equilibria $\mathbb{E}$ for PDE (3.1).

3.1. Spectrum at each equilibrium We explore the spectrum about every equilibria in $\mathbb{E}$ as the spectrum is crucial in identifying the existence and properties of invariant manifolds/subspaces. Since the cell PDE (3.1) is linear, the perturbation problem is identical at every U, namely (3.1) itself.

EXAMPLE 3.2. Consider the case where the heterogeneity κ is constant. In the vector space $\mathbb{H}_C$, and upon defining wavenumbers $k_i = 2\pi/\ell_i$, a complete set of linearly independent eigenfunctions of the right-hand side of (3.1) are $e^{i(mk_1 x_1 + nk_2 x_2)}$ for every integer m, n. The spectrum of eigenvalues is then $\lambda_{mn} = -\kappa(mk_1 + nk_2)^2$. This spectrum has one zero-eigenvalue and the rest are negative: $\lambda_{mn} \leq -\kappa k_1^2 < 0$ (recall $\ell_1 > \ell_2$ so $k_1 < k_2$).

For general heterogeneity κ satisfying Assumption 3.1, we here establish that the cell eigenvalue problem associated with (3.1) is self-adjoint, and hence has only real eigenvalues. Denote the right-hand side operator as $\mathcal{L}_0 := (\partial_{x_1} + \partial_{x_2})\{\kappa(x_1, x_2)(\partial_{x_1} + \partial_{x_2})\}$ to be solved with ℓ_i-periodic boundary conditions in x_i. Also, we use the inner product $\langle \mathfrak{u}, \mathfrak{v} \rangle := \iint_C \mathfrak{u}\bar{\mathfrak{v}}\, dx_1\, dx_2$ over the rectangular cross-section $C := [0, \ell_1] \times [0, \ell_2]$, where an overbar denotes complex conjugation. Then, for every pair of functions $\mathfrak{u}, \mathfrak{v} \in \mathbb{H}_C$, consider

$$
\begin{aligned}
\langle \mathcal{L}_0 \mathfrak{u}, \mathfrak{v} \rangle &= \iint_C \bar{\mathfrak{v}}(\partial_{x_1} + \partial_{x_2})\{\kappa(\mathfrak{u}_{x_1} + \mathfrak{u}_{x_2})\}\, dx_1\, dx_2 \\
&= \iint_C \bar{\mathfrak{v}}\partial_{x_1}\{\kappa(\mathfrak{u}_{x_1} + \mathfrak{u}_{x_2})\} + \bar{\mathfrak{v}}\partial_{x_2}\{\kappa(\mathfrak{u}_{x_1} + \mathfrak{u}_{x_2})\}\, dx_1\, dx_2 \\
&= \int_0^{\ell_2} \left\{ [\bar{\mathfrak{v}}\kappa(\mathfrak{u}_{x_1} + \mathfrak{u}_{x_2})]_0^{\ell_1} - \int_0^{\ell_1} \bar{\mathfrak{v}}_{x_1}\kappa(\mathfrak{u}_{x_1} + \mathfrak{u}_{x_2})\, dx_1 \right\} dx_2 \\
&\quad + \int_0^{\ell_1} \left\{ [\mathfrak{v}\kappa(\mathfrak{u}_{x_1} + \mathfrak{u}_{x_2})]_0^{\ell_2} - \int_0^{\ell_2} \bar{\mathfrak{v}}_{x_2}\kappa(\mathfrak{u}_{x_1} + \mathfrak{u}_{x_2})\, dx_2 \right\} dx_1 \\
&= -\iint_C (\bar{\mathfrak{v}}_{x_1} + \bar{\mathfrak{v}}_{x_2})\kappa(\mathfrak{u}_{x_1} + \mathfrak{u}_{x_2})\, dx_1\, dx_2,
\end{aligned}
$$

as the boundary contributions vanish due to the ℓ_i-periodicity. Reverse the above steps with the roles of $\mathfrak{u}$ and $\mathfrak{v}$ swapped, to then deduce $\langle \mathcal{L}_0 \mathfrak{u}, \mathfrak{v} \rangle = \langle \mathfrak{u}, \mathcal{L}_0 \mathfrak{v} \rangle$. Thus, the operator $\mathcal{L}_0$ is self-adjoint.

Consequently, every eigenvalue is real and the eigenvectors are pairwise orthogonal (or may be chosen to be so).

The next step is to establish that all the nonzero eigenvalues of $\mathcal{L}_0$ are negative and bounded away from zero. Consider the eigen-problem $\mathcal{L}_0 \mathfrak{v} = \lambda \mathfrak{v}$ for cross-sectional structures $\mathfrak{v} \in \mathbb{H}_C$. Apply $\langle \cdot, \mathfrak{v} \rangle$ to the eigen-problem to see that

$$
\begin{aligned}
\lambda \langle \mathfrak{v}, \mathfrak{v} \rangle &= \iint_C \bar{\mathfrak{v}} (\partial_{x_1} + \partial_{x_2}) \{ \kappa (\mathfrak{v}_{x_1} + \mathfrak{v}_{x_2}) \} \, dx_1 \, dx_2 \\
&= \cdots = - \iint_C \kappa |\mathfrak{v}_{x_1} + \mathfrak{v}_{x_2}|^2 \, dx_1 \, dx_2 \\
&\leq -\kappa_{\min} \iint_C |\mathfrak{v}_{x_1} + \mathfrak{v}_{x_2}|^2 \, dx_1 \, dx_2 ,
\end{aligned}
$$

via integration by parts and the ℓ_i-periodic conditions in x_i. To deduce an upper bound on the nonzero eigenvalues λ, let us minimize $\iint_C |\mathfrak{v}_{x_1} + \mathfrak{v}_{x_2}|^2 \, dx_1 \, dx_2$ in $\mathbb{H}_C$ subject to $\langle \mathfrak{v}, \mathfrak{v} \rangle = \iint_C |\mathfrak{v}|^2 \, dx_1 \, dx_2 = 1$ and that $\mathfrak{v}(x_1, x_2)$ has zero mean (being orthogonal to the constant eigenvector corresponding to $\lambda = 0$). Introduce a Lagrange multiplier μ, and use calculus of variations to minimize $\iint_C |\mathfrak{v}_{x_1} + \mathfrak{v}_{x_2}|^2 \, dx_1 \, dx_2 + \mu(\iint_C |\mathfrak{v}|^2 \, dx_1 \, dx_2 - 1)$. Via integration by parts, it follows that a minimizer must satisfy $(\partial_{x_1} + \partial_{x_2})^2 \mathfrak{v} = -\mu \mathfrak{v}$ over $\mathfrak{v} \in \mathbb{H}_C$. This is the problem Example 3.2 solves, giving potential minimizers as $e^{i(mk_1x_1 + nk_2x_2)}$ for multiplier $\mu = (mk_1 + nk_2)^2$. The zero mean condition requires at least one of m, n nonzero, and since $\ell_1 > \ell_2$, so minima are thus linear combinations of $e^{imk_1x_1}$ for $m = \pm 1$. These give $\iint_C |\mathfrak{v}_{x_1} + \mathfrak{v}_{x_2}|^2 \, dx_1 \, dx_2 / \langle \mathfrak{v}, \mathfrak{v} \rangle = k_1^2 = 4\pi^2/\ell_1^2$. Hence, we obtain the upper bound on the nonzero eigenvalues of $\lambda \leq -\beta_1$ for $\beta_1 = 4\pi^2 \kappa_{\min}/\ell_1^2$.

In the case of the heterogeneous wave propagation problem, $u_{tt} = \partial_x \{ \kappa(x) u_x \}$, this subsection's eigenvalue analysis establishes that for the cross-sectional dynamics, there exists a zero eigenvalue separated from pure imaginary eigenvalues of magnitude at least $\sqrt{\beta_1} = 2\pi \sqrt{\kappa_{\min}}/\ell_1$.

3.2. Results of slowly varying theory Let us comment on the preconditions for the next Proposition 3.3 as listed in [52, Assumption 2]. First, Section 3.1 establishes that the spectrum of $\mathcal{L}_0$ is as required for the Hilbert space $\mathbb{H}_C$. Hence, we decompose the space into two closed $\mathcal{L}_0$-invariant subspaces, the (slow) centre $\mathbb{E}_c^0$ and the stable $\mathbb{E}_s^0$. Since the operator $\mathcal{L}_0$ is self-adjoint, it generates the required strongly continuous semigroups in the Sobolev space $\mathbb{H}_C$ [13, Ch. 6]. Hence, the following result holds for homogenization.

PROPOSITION 3.3 (Homogenization exists and emerges). *By* [52, *Proposition 6*], *for every chosen truncation order N, in a domain $\mathbb{X}$ of 'slowly varying solutions' and after the decay of transients $O(e^{-\beta't})$ for $\beta' \approx \beta_1$, the mean field $U(t, x) := (\ell_1 \ell_2)^{-1} \iint_C \mathfrak{u}(t, x, x_1, x_2) \, dx_1 \, dx_2$ satisfies a generalized homogeneous PDE*

$$\frac{\partial U}{\partial t} = \sum_{n=0}^{N} K_n \frac{\partial^n U}{\partial x^n}, \quad x \in \mathbb{X} \subset [0, L], \tag{3.2}$$

in terms of some deterministic constants K_n, to a quantifiable error [52, (9)–(10) and (23)].

The above mentioned error [52, (23)] involves too many new parameters to meaningfully detail here—but typically, the most important factor at each and every location $x = x_0$ is the $(N + 1)$th spatial derivative of the field u in a spatial neighbourhood of x_0. The open subset $\mathbb{X}$ of the domain $[0, L]$ is then that part of the domain where the error in (3.2) [52, (23)], dominantly $\partial_x^{N+1} u$, is small enough for the modelling purposes at hand.

Also, using the specific mean field defined in Proposition 3.3—the usual "cell average"—is optional: one may instead parametrize the macroscale slow manifold in terms of any reasonable alternative amplitude [53, Section 5.3.3].

A generating function argument [52, Corollaries 12 and 13] establishes that classic, formal, 'slowly varying' analyses of the embedding PDE (2.1) are valid. One just needs to formally treat derivatives in the 'large' direction, $\partial/\partial x_0$, as 'small' in a consistent asymptotic sense [50, 46].

3.3. Wave propagation in heterogeneous media

In the case of the heterogeneous wave propagation problem, $u_{tt} = \partial_x\{\kappa(x)u_x\}$, I conjecture that a backwards approach [32, 54] to the slowly varying theory here would support a cognate version of Proposition 3.3 about the generalized homogeneous wave PDE $U_{tt} = \sum_{n=0}^{N} K_n \partial_x^n U$ describing its dispersive macroscale waves.

However, in this case of heterogeneous wave propagation in heterogeneous media, the slow manifold is no longer attractive/emergent (unless there is some significant perturbing dissipative mechanism not included in the ideal wave PDE). Instead, we expect that the slow manifold acts as a 'centre' for any fast oscillations arising from the initial conditions. Indeed, conjectured backwards theory [54, Section 2.5] would more precisely assert that there is a system 'close' to the given physical PDE $u_{tt} = \partial_x\{\kappa(x)u_x\}$ (close to some specified order in some sense) that precisely possesses the constructed homogeneous slow manifold for the macroscale, and that precisely acts as a centre for all nearby dynamics. In this way, the backwards theory would straightforwardly establish accurate modelling over "time scales $O(\varepsilon^{-\alpha})$" [1, 24], typically for exponent $\alpha = N$, the order of truncation.

Although this article addresses homogenization of *linear* systems, a comment about homogenizing *nonlinear* wave systems is appropriate here. As geophysical fluid dynamists have understood for decades, for any given wave system, it is common that a nonlinear slow manifold, such as homogenization seeks, cannot actually exist [36]. Nonetheless, backwards theory [32, 54] potentially applies to establish that there exists a wave system 'close' to the specified nonlinear wave system, where the 'close' systems precisely possess the constructed nonlinear slow manifold and the constructed

evolution thereon. Thus, the dynamical systems approach developed here provides a methodology to prevail over subtleties in homogenizing nonlinear wave problems.

4. Example construction of any-order homogenized PDEs

Corollary 13 of [52] established that a procedure [46], previously viewed as formal, is indeed a rigorous method to construct the slow manifold modelling PDEs (3.2). Here we use the computer algebra system (CAS) version of the procedure [50], as detailed in generality and examples of the book [53, Part III].

Appendix A lists and documents the computer algebra code. The code constructs the homogenization for the case of heterogeneity,

$$\kappa(x_1, x_2) := 1/[1 + a_1 \cos k_1 x_1 + a_2 \cos k_2 x_2], \tag{4.1}$$

in terms of microscale wavenumbers $k_i = 2\pi/\ell_i$ for the given microscale periodicities ℓ_1, ℓ_2. We write approximations to the slow manifold model of the embedding PDE (2.1) in terms of a 'mean' field $U(t, x)$ that evolves according to an homogenized PDE of the form (3.2).

Quickly verify an approximation. First, Appendix A.1 verifies that an approximate field is

$$\mathfrak{u}(t, x, x_1, x_2) = U + (a_1/k_1 \sin k_1 x_1 + a_2/k_2 \sin k_2 x_2)\frac{\partial U}{\partial x}$$

$$+ (a_1/k_1^2 \cos k_1 x_1 + a_2/k_2^2 \cos k_2 x_2)\frac{\partial^2 U}{\partial x^2} + \cdots \tag{4.2a}$$

such that the mean field U evolves according to the homogenized PDE

$$\frac{\partial U}{\partial t} = \frac{\partial^2 U}{\partial x^2} + \cdots \tag{4.2b}$$

(the coefficient 1 of the mean diffusivity is the classic harmonic mean of the specific heterogeneous diffusivity (4.1)). To verify, substitute (4.2) into the governing PDE (2.1) and find the PDE's residual contains only terms in U_{xxx} and higher derivatives. We denote this by saying that the residual is zero to an error $O(\partial_x^3)$. Since the PDE residual is $O(\partial_x^3)$, then theory [52, Proposition 6] assures us that the derived slow manifold and its evolution (4.2) is correct to error $O(\partial_x^3)$.

4.1. Iteration systematically constructs approximations   To construct approximations systematically, we repeatedly compute the residual, which then drives corrections, until the residual is zero to any specified order of error. Theory then assures us that the slow manifold is approximated to the same order of error [52]. For example, the CAS iteratively constructs the improved homogenization (the so-called 'fourth-order' case $N = 6$) that

$$\frac{\partial U}{\partial t} = \frac{\partial^2 U}{\partial x^2} + \frac{1}{2}(a_1^2/k_1^2 + a_2^2/k_2^2)\frac{\partial^4 U}{\partial x^4}$$

$$+ \left[\frac{1}{2}(a_1^2/k_1^2 + a_2^2/k_2^2)^2 - 2(a_1^2/k_1^4 + a_2^2/k_2^4)\right]\frac{\partial^6 U}{\partial x^6} + O(\partial_x^7). \qquad (4.3)$$

The code of Appendix A.2 constructs this 'fourth-order' homogenization (4.3), and executes in approximately 26 seconds. In the case of the heterogeneous wave propagation problem, $u_{tt} = \partial_x\{\kappa(x)u_x\}$, we expect the macroscale homogenized dispersive wave PDE to have U_{tt} equal to the same right-hand side as the above. Most other rigorous homogenizations invoke a limit '$\epsilon \to 0$' for some defined scale separation parameter such as $\epsilon = \ell_1/L$. Here such a limit corresponds to the scale separation limit $k_1, k_2 \to \infty$, in which case, the homogenization (4.3) reduces to the classic, simple, diffusion PDE $U_t = U_{xx}$. However, I emphasize that our homogenized PDEs like (4.3) are established for the finite scale separation of real physical materials: finite ϵ, k_1, k_2.

In use, any specific truncation of higher-order homogenization, such as (4.3), may need some asymptotically consistent regularization [7, Section 2]. For an example of regularization, let us suppose we decide on the $N = 4$ truncation $U_t = U_{xx} + \alpha^2 U_{xxxx}$ with derived parameter $\alpha := \sqrt{(a_1^2/k_1^2 + a_2^2/k_2^2)/2}$. The fourth derivative term, $+\alpha^2 U_{xxxx}$ is undesirably destabilizing. However, to the same order of error, namely $O(\partial_x^6)$, the chosen truncation is asymptotically equivalent to the regularized equation $U_t = (1 - \alpha^2\partial_x^2)^{-1}U_{xx}$. This regularization may be alternatively written as

$$(1 - \alpha^2\partial_x^2)U_t = U_{xx}, \quad \text{or} \quad U_t = \frac{1}{2\alpha}e^{-|x|/\alpha} \star U_{xx}.$$

The spatially nonlocal convolution $e^{-|x/\alpha|}\star$, whether explicit or implicit, stabilizes the regularized chosen truncation while preserving asymptotic consistency [41, cf. Section 2.2]. Such nonlocal PDEs have previously been found desirable in various homogenizations of heterogeneous systems [17, pp. 2–3].

Optional high-order construction. We may set $a_2 = 0$ to get simpler results for a single periodic component in the heterogeneity, namely $\kappa(x_1) = 1/[1 + a_1 \cos k_1 x_1]$. In this case, it becomes feasible to construct the homogenization to high-order, $N = 34$, in spatial derivatives. To construct expressions that are exact in heterogeneity amplitude a_1, we also need to construct to the same order in a_1 because the evidence is that here, the expansions in heterogeneity amplitude a_1 truncate at just less than the same order as the order of derivatives. For this option (Appendix A.2), the algebra of order $N = 34$ takes roughly one minute of compute time.

In general. The code of Appendix A.2 assumes the heterogeneity $\kappa \approx 1$, specifically, $\kappa = 1/[1 + \kappa']$ for some $\kappa' \propto a$. Then multiplication by κ is realized as multiplication by $\sum_{n=0}^{N-1}(-\kappa')^n$.

The method [50] is to start the iteration with the leading 'trivial' approximation for the field and its evolution: that is, $u \approx u^{(1)} := U$ such that $\partial U/\partial t \approx g^{(1)} := 0$. Then the nth iteration is given approximations $u^{(n)}$ and $g^{(n)}$, and starts by evaluating, via the flux $f^{(n)} := -\kappa(u_x^{(n)} + u_{x_1}^{(n)} + u_{x_2}^{(n)})$, and then the residual of the embedding PDE (2.1):

$$\mathrm{Res}^{(n)} := u_t^{(n)} + f_x^{(n)} + f_{x_1}^{(n)} + f_{x_2}^{(n)}.$$

First update the evolution via the solvability integral that here is the mean over x_1, x_2: $g^{(n+1)} := g^{(n)} + g'$, where $g' := \overline{\mathrm{Res}^{(n)}}$. Second, update the field by a correction u' through using two steps to solve $(\partial_{x_1} + \partial_{x_2})[\kappa(u'_{x_1} + u'_{x_2})] = \mathrm{Res}^{(n)} + g'$: step 1 integrates to solve $v_{x_1} + v_{x_2} = \mathrm{Res}^{(n)} + g'$ with zero mean to avoid unbounded updates; and step 2 integrates again to solve $u'_{x_1} + u'_{x_2} = v/\kappa$ with zero mean. This second "zero mean" ensures preservation of our *free choice* that the macroscale field parameter U is to be the local mean of the microscale field u. Then update the field approximation with $u^{(n+1)} := u^{(n)} + u'$.

The iterative loop terminates when the PDE residual $\mathrm{Res}^{(n)}$ is zero to the specified orders of error. Then the constructed homogenization, such as (4.2) and (4.3), is correct to the same order [52, Proposition 6].

Analogy with machine learning. The recursive iteration used in the above construction was originally developed nearly 30 years ago [50]. Let us draw an analogy between this iteration and machine learning algorithms where an AI learns the generic form of the macroscale evolution from many thousands of simulations [28, 29, 35]. In the algorithm here, each recursive iteration is analogous to a layer in a deep neural network, evaluating residuals is analogous to a nonlinear neuronal function, and the linear update corrections are analogous to using weighted linear combination of outputs of one layer as the inputs of the next layer. However here, the recursion is a 'smart neural network' in that both the neurons and the 'linear weights' are crafted to the problem at hand using the physics encoded in the PDE operator—they are 'physics-informed'. Further, being analytic, a single analysis encompasses all 'data points' in the state space's domain (here all 'slowly varying' functions in $\mathbb{H}_{\mathcal{D}}$), not just a finite sample as in machine learning (possibly a biased sample). Consequently, via such algorithms, I contend that mathematicians have for decades been using such recursive iteration for implementing smart analogues of machine learning. Such analytic learning empowers the physical interpretation, validation and verification required by modern science [10].

4.2. Numerics verify these homogenizations   For a computational verification, let us use the specific instance of the heterogeneity (4.1) with $a_1 = a_2 = 0.4$, and wavenumbers $k_1 = 21$ and $k_2 = 34$, that is, microscale lengths are $\ell_1 = 2\pi/k_1 \approx 0.30$ and $\ell_2 = 2\pi/k_2 \approx 0.18$ (all nondimensional). Consequently, let the macroscale then refer to lengths $\gtrsim 2\ell_1 \approx 0.6$ (Section 5), that is, wavenumbers $|k| \lesssim 10$. We compare the macroscale characteristics of the right-hand side of the homogenized (4.3) with the right-hand side of the original heterogeneous PDE (1.1).
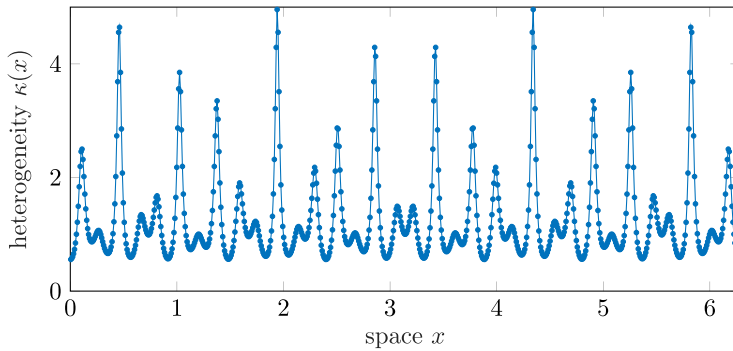
FIGURE 2. Example (near) quasi-periodic microscale heterogeneous coefficient (4.1) for the case of $a_1 = a_2 = 0.4$ and wavenumbers $k_1 = 21$ and $k_2 = 34$.

Here the microscale heterogeneity (4.1) (see Figure 2), is near-quasi-periodic with $k_2/k_1 = 1.6190 \approx (\sqrt{5} + 1)/2$, although this heterogeneity does have a large macroscale period 2π (as plotted). Consequently, numerically, we solve heterogeneous PDE (1.1) on the domain of length $L = 2\pi$ with a microgrid of 714 points, $\delta x = 0.0088$. The "numeric" column of Table 1 gives the resultant eigenvalues of the full heterogeneous PDE (1.1) for macroscale wavenumbers k, $|k| < 10$. These eigenvalues reflect either the decay rate of the diffusion problem (1.1) or the square of frequencies for the corresponding wave problem (1.3). The homogenization (4.3) of this quasi-periodic heterogeneity may be truncated at any chosen order in ∂_x, so we compare its predictions for three truncations: the usual leading order homogenization with truncation to errors $O(\partial_x^3)$; the 'second-order' homogenization with errors $O(\partial_x^5)$; and the 'fourth-order' homogenization with errors $O(\partial_x^7)$. We simply substitute the mode $U = e^{\lambda t + ikx}$ into the truncated right-hand side of (4.3) to obtain rates to compare with that of the full problem. Table 1 shows the two expected results: first, for each wavenumber, the accuracy increases with order of truncation; and second, for each order, as the macroscale wavenumber becomes larger (the macroscale length of the mode decreases), the error increases. These expected trends in the errors are shown clearly in Figure 3 that plots the relative errors on log–log axes[1]. Table 1 and Figure 3 verify our approach to modelling the homogenized dynamics of quasi-periodic heterogeneous problems.

Figure 3 indicates that the homogenization errors become large for wavenumbers $|k| \gtrsim 10 \approx k_1/2$. This apparent limit of the resolvable wavenumbers matches the estimate obtained in Section 5, the lower bound (5.1), that the macroscale lengths resolved by the homogenization are longer than roughly twice ℓ_1.

---

[1]Figure 3 is truncated to a minimum relative error of 10^{-4}, because the spatial discretization of the full PDE (1.1) has discretization errors $O(\delta x^2)$ which lead to its computations naturally having errors of approximately 10^{-4}.

TABLE 1. Macroscale eigenvalues as a function of macroscale wavenumber k: the "numeric" column lists the computed eigenvalues of (1.1) for spatial discretization $\delta x = 0.0088$; the last three columns are the rates predicted for $U = e^{ikx}$ by the homogenization (4.3) truncated to errors $O(\partial_x^{n+1})$ for orders $n = 2, 4, 6$, respectively.

k	numeric	2nd	4th	6th
1	−0.9997	−1	−0.9997	−0.9997
2	−3.9958	−4	−3.9960	−3.9959
3	−8.9777	−9	−8.9797	−8.9784
4	−15.9251	−16	−15.9358	−15.9286
5	−24.8042	−25	−24.8434	−24.8159
6	−35.5486	−36	−35.6752	−35.5931
7	−48.0433	−49	−48.3983	−48.1913
8	−61.9891	−64	−62.9735	−62.5123
9	−76.5772	−81	−79.3557	−78.4208
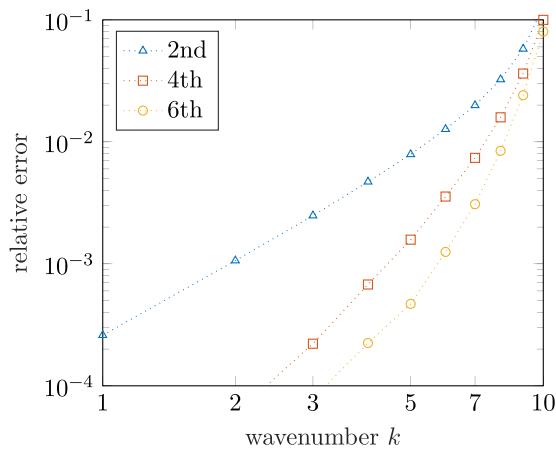
FIGURE 3. Relative errors in the macroscale predictions by the three truncations of the homogenized PDE (4.3). Table 1 gives the data underlying this plot of errors. These are for the quasi-periodic heterogeneity (4.1) with $a_1 = a_2 = 0.4$ and wavenumbers $k_1 = 21$ and $k_2 = 34$.

5. Spatial resolution of high-order homogenization

An homogenized PDE, such as (3.2) and (4.3), accurately predicts the evolution of the mean field $U(t, x)$ *provided* that, on the scale of the heterogeneity, the spatial gradients are sufficiently small, that is, provided the solutions are sufficiently slowly varying in space. Matous et al. [38, Section 3.2] phrased the proviso as "the scale of the microstructural fluctuations, $[\ell_1]$, must be ... much smaller than the macroscopic field fluctuations, ℓ_M" (expressed similarly by Nguyen et al. [43, Section 2.2.2]). The following question arises: what does "sufficiently small", "sufficiently slowly varying"

or "much smaller" actually mean physically? This section provides an indicative *quantitative* answer.

Here we show that in a prototypical family of homogenization problems, we only need to require that the

$$\text{macroscale lengths } \ell_M \gtrsim 2\ell_1. \tag{5.1}$$

This lower bound on the macroscale lengths is approximate and indicative because the actual performance of an homogenization depends upon the details of the heterogeneity κ, a chosen truncation N of the homogenized PDE, any chosen specific regularization of the PDE, the chosen desired error of predictions and so on. Recall that this lower bound (5.1) agrees with the growth of errors seen in the example of Figure 3. However here, the numerical coefficient 2 in (5.1) arises from a well-established quantitative procedure.

Such a result contrasts with the prevailing expectation provided by other homogenization frameworks: for example, Allaire et al. [3, p. 2] comment "no convergence is expected".

The procedure we invoke is that of high-order asymptotic construction followed by Domb–Sykes plots [22, 67] or Mercer–Roberts plots [40, Appendix] that estimate the distance to the nearest, convergence limiting, singularity in the series approximations. We analyse an homogenized PDE (3.2) and (4.3) by considering its corresponding Fourier transform ($\partial_x \leftrightarrow ik$): $\partial \tilde{U}/\partial t = \sum_{n=0}^{\infty} (ik)^n K_n \tilde{U}$ in terms of the Fourier transform $\tilde{U}(t, k)$ of the mean field $U(t, x)$. Then the coefficient $\mathcal{K}(k) := \sum_{n=0}^{\infty} (i^n K_n) k^n$ is a series in wavenumber k. If we can show convergence for $|k| < k_*$ for some wavenumber bound k_*, then we deduce that the homogenized PDE is valid for spatial structures of length scale $\ell_M > 2\pi/k_*$. We know that the radius of convergence k_* is the distance to the singularity of $\mathcal{K}(k)$ nearest the origin ($k = 0$). However, we only know N terms in the series for $\mathcal{K}(k)$, so Domb–Sykes and Mercer–Roberts plots estimate the distance k_* by extrapolating the 'ratio test' from finite n to infinity, in the cases of a single singularity or a complex conjugate pair of singularities, respectively. For example, this technique has been used to quantitatively predict the spatial limit on PDEs modelling shear dispersion in channels and pipes [40, 41]. Figure 4 is an example Mercer–Roberts plot for one homogenization case developed here. The extrapolations to $1/n = 0$ ($n \to \infty$) in the figure indicate that the convergence is limited by a complex conjugate pair of singularities at a distance in wavenumber space of $k_* \approx 1/\sqrt{3.6} \approx 0.52$.

To obtain such plots and estimates, we need to compute the homogenization series (3.2) and (4.3) to high-order. For the case of quasi-periodic heterogeneity, the algebraic complexity explodes combinatorially with increasing order. Consequently, as a representative example, we explore the accessible case of homogenization with a single microscale period, specifically the heterogeneity
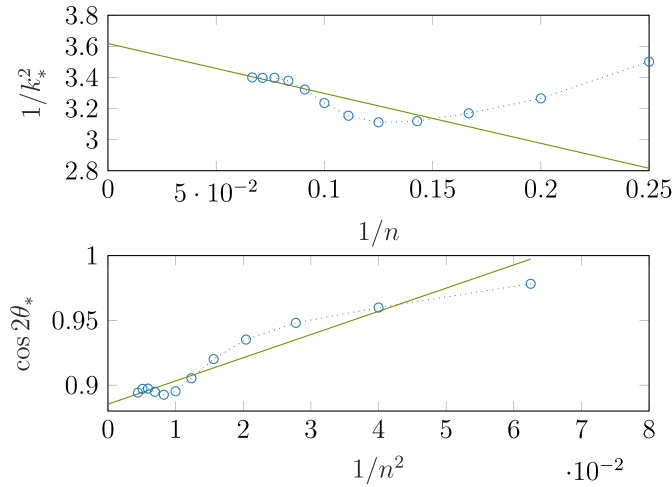
$$\kappa(x) := 1/[1 + a \cos x]. \tag{5.2}$$

FIGURE 4. Macroscale wavenumbers k of convergence are estimated from Mercer–Roberts plots [40, Appendix] for the series $\mathcal{K}(k)$ in the case of heterogeneity (5.2), here with $a = 0.975$. We use the first 17 terms of the series in k^2. Extrapolation to $1/n = 0$ estimates the location of a pair of complex conjugate singularities that limit the radius of convergence.

The computer algebra code overviewed in Section 4 constructs the homogenization in this case via the option of setting $a_2 = 0$, $a_1 = a$ and $k_1 = 1$. For algebraic simplicity, in this case, the analysis is nondimensionalized on the microscale length so that nondimensionally, the microscale period $\ell_1 = 2\pi$. Executing the code with this option gives that the homogenized PDE (3.2) begins with

$$U_t = [\partial_x^2 + \tfrac{1}{2}a^2\partial_x^4 + (-2a^2 - \tfrac{1}{4}a^4)\partial_x^6 + (8a^2 - \tfrac{135}{32}a^4 + \tfrac{5}{8}a^6)\partial_x^8$$
$$+ (-32a^2 + \tfrac{879}{32}a^4 - \tfrac{261}{32}a^6 + \tfrac{7}{8}a^8)\partial_x^{10} + O(\partial_x^{12})]U. \tag{5.3}$$

As a first step in investigating such high-order homogenization, observe that the a^2 terms are evidently all of the form

$$\tfrac{1}{2}a^2\partial_x^4(-4\partial_x^2)^{n/2-2}$$

(this form holds up to at least order $n = 34$). Hence, in Fourier space ($\partial_x \leftrightarrow ik$), the PDE (5.3) becomes the series for[1]

$$\tilde{U}_t = [-k^2 + \tfrac{1}{2}a^2k^4/(1 - 4k^2) + O(a^4)]\tilde{U}.$$

The divisor $(1 - 4k^2)$ in this expression indicates that for small heterogeneity amplitude a, the wavenumbers resolvable by such an homogenization series are limited by the pole singularities at $k = \pm 1/2$, that is, a bound on the convergence of the series

---

[1]Incidentally, multiplying by $(1 - 4k^2)$ and taking the inverse Fourier transform, this establishes that the PDE $(1 + 4\partial_{xx})U_t = U_{xx} + (4 + a^2/2)U_{xxxx}$, since the PDE's error is simply $O(a^4)$, is an accurate and stable homogenization for all (non-dimensional) wavelengths longer than $4\pi\sqrt{1 + a^2/8}$.
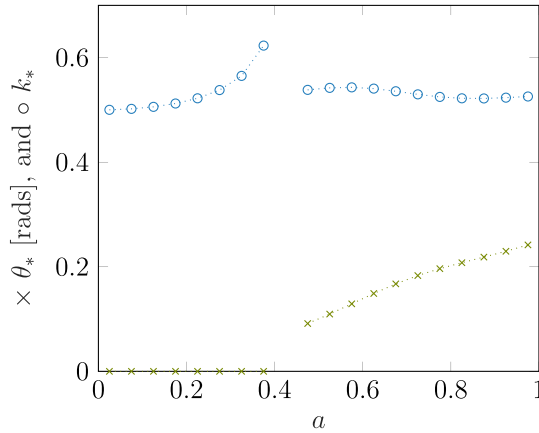
FIGURE 5. In complex wavenumber space, plot estimates of the radius k_* (circles) and angle θ_* (crosses) of the convergence limiting singularity of the homogenization (5.3) as a function of the heterogeneity amplitude a in (5.2). The estimates around $a \approx 0.4$ are unreliable (see text).

is $k_* = 1/2$. Hence, for small a, the homogenized PDE (5.3) potentially resolves all wavelengths longer than $\ell_* := 2\pi/k_* = 4\pi = 2\ell_1$[1].

I conjecture that the singularities at wavenumber $k = \pm1/2$ are connected to, in wave propagation through heterogeneous media, the well-known phenomenon of spectral gaps, namely frequencies at which no wave can propagate through the underlying medium [17, p. 2].

Figure 5, for small a, confirms this bound on the wavenumbers and wavelengths. The estimates plotted in Figure 5 are obtained from Section 4 constructing the series (5.3) to errors of order 35 in ∂_x, or equivalently to errors $O(k^{35})$. This CAS construction provides us with the first 17 nonzero coefficients in the series in k^2 for $\mathcal{K}(k)$.

- For heterogeneity amplitude $a \lesssim 0.4$, these coefficients have the same sign. Consequently, Domb–Sykes plots [22, 67], akin to the top panel of Figure 4, predict convergence limiting singularities at real $k = \pm k_*$ as shown in the left-part of Figure 5.
- For heterogeneity amplitude $a \gtrsim 0.4$, the coefficients have a more complicated sign pattern, indicating the convergence limiting singularity is now a complex conjugate pair in the complex k^2-plane. Mercer–Roberts plots [40, Appendix], such as Figure 4, estimate the radius and angle of these convergence limiting singularities as shown in the right-part of Figure 5.

The two distinct behaviours summarized in Figure 5 are likely due to singularities moving as a function of heterogeneity parameter a. We conjecture that for $a \lesssim 0.3$,

---

[1]The limit $a \to 0$ is nonuniform. At $a = 0$, there is no heterogeneity and the 'homogenized' PDE (1.2) is precisely the original PDE (1.1), and therefore valid for *all* wavelengths and wavenumbers. Whereas for small nonzero a, the singularities at wavenumber $k = \pm1/2$ persist and limit validity for small a—it is just that the singularities have a strength $O(a^2)$ that vanishes as $a \to 0$.

there is a second real singularity for wavenumbers larger than k_*. As a increases, both these singularities move and appear to collide for $a \approx 0.35$. After collision, they separate and move out into the complex k plane ($a \gtrsim 0.4$). The Domb–Sykes and Mercer–Roberts estimates are both unreliable near such collision, so the estimates for $a \approx 0.3$ to ≈ 0.4 are unreliable. With this caveat, the evidence of Figure 5 indicates that across all $0 < a < 1$, our homogenization can resolve all wavenumbers $|k| < 1/2$. That is, high-order homogenization can resolve wavelengths longer than just twice the wavelength of the underlying periodicity.

In the case of the heterogeneous wave propagation problem, $u_{tt} = \partial_x\{\kappa(x)u_x\}$, we expect the same restrictions on the spatial resolution because we expect the right-hand side of PDE (4.3) to remain the same for the homogenized waves.

The case of quasi-periodic heterogeneity. In the case of the quasi-periodic heterogeneity (4.1), observe in the homogenization PDE (4.3) that the coefficients in a_i are divided by wavenumbers k_i, and with increasing powers of k_i as the order increases. This suggests that higher-order terms in the series are dominated by the smallest wavenumber k_i, namely k_1. That is, the higher-order terms should be dominated by the longest microscale heterogeneity, here that of $a_1 \cos(k_1 x)$. Hence, we expect the limiting wavenumber and wavelengths to be the same as those for the single periodic heterogeneity (5.2). Consequently, expect the bound (5.1) to be valid for this quasi-periodic heterogeneity.

Temporal resolution. The above exploration finds that the spatial resolution of the homogenization appears to vary little with heterogeneity strength a. The temporal resolution is quite a different issue, and it may depend significantly upon a. For example, Figure 4 comes from the case $a = 0.975$, where the microscale heterogeneity varies by a factor of 80 across a microscale period. In similar scenarios, the time scale of decay to the homogenized model, roughly $1/\beta_1 = \ell_1^2/(4\pi^2 \kappa_{\min})$ (end of Section 3.1), may be several orders of magnitude longer than for small heterogeneity. For valid predictions by the homogenization, the macroscale time scale of interest needs to be longer than that of this decay.

Of course, all equilibrium problems satisfy this temporal bound.

6. Three-scale homogenization

There is interest in physical systems possessing a microscale, a mesoscale and a macroscale [21, 45]. Such three-scale systems are encompassed in the framework of Section 2 when $\ell_2 \ll \ell_1 \ll L$. That is, the cylindrical domain of Figure 1 is shaped like a physical ruler in that the domain is significantly thinner vertically than its width, and its width is in turn significantly thinner than its length. Although Section 5 finds that these length ratios need to be at least two, they are not necessarily much bigger.

In this scenario, the arguments of Section 2 still apply: we solve the phase-shift embedding PDE (2.1) to obtain solutions of the heterogeneous PDEs (1.1) and (2.2). It is the slow manifold support and analysis that differs in detail.

Because this rigorous homogenization could, in principle, be exact at finite scale separation, we find here the expected result that a slow manifold homogenization of a 'meso-slow' manifold homogenization of the microscale system is the same as the slow manifold homogenization of the microscale (Sections 3 and 4). That is, in principle, this approach to homogenization is transitive.

The same transitivity of homogenization would also hold in the case of the heterogeneous wave propagation problem, $u_{tt} = \partial_x\{\kappa(x)u_x\}$.

6.1. Meso-slow homogenization To analyse the heterogeneous PDEs (1.1) and (2.2) as a three-scale system, we first establish and create the 'meso-slow' manifold homogenization. That is, we use that the domain $\mathcal{D}$, Figure 1, is thin in x_2, that is, $\ell_2 \ll \ell_1, L$. Consequently, we consider the embedding PDE (2.1) by assuming the spatial variations in both x_0 and x_1 are on a relatively large length scale. That is, the derivatives of $\mathfrak{u}$ and κ in both x_0 and x_1 are treated as small.

This homogenization is an example of that of a functionally graded material [5], because the mesoscale variations in heterogeneity in x_1 are on a length scale $\ell_1 \gg \ell_2$. Our slow manifold approach systematically incorporates all such variations within the analysis: for example, giving the fourth-order homogenization (6.3)–(6.4). At orders higher than the leading order, we systematically find higher-order derivatives of the larger scale material structure: for example, the fourth-order coefficient in the upcoming PDE (6.4) involves the third derivative $\mathfrak{K}'''(x_1)$ of the mesoscale variations. This approach automatically incorporates effects obtained by the "second-order homogenization" of Anthoine [5].

Akin to Section 3, we here establish the basis of a slow manifold. Consider PDE (2.1), with $\partial/\partial x_0$ and $\partial/\partial x_1$ neglected, and in the Sobolov space $\mathbb{H}_{[0,\ell_2]}$ with ℓ_2-periodic boundary conditions in x_2:

$$\frac{\partial \mathfrak{u}}{\partial t} = \frac{\partial}{\partial x_2}\left\{\kappa(x_1, x_2)\frac{\partial \mathfrak{u}}{\partial x_2}\right\}. \tag{6.1}$$

The basis established here applies at each and every x_0, x_1.

Equilibria. For the cell PDE (6.1), and for every x_0, x_1, in $\mathbb{H}_{[0,\ell_2]}$, clearly $\mathfrak{u}(t, x_2) = \mathfrak{U}$, constant in x_2, forms a subspace of equilibria $\mathbb{E}$.

Spectrum identifies invariant manifolds. Since the cell PDE (6.1) is linear, the perturbation problem is identical at every equilibria in $\mathbb{E}$, namely (6.1) itself. We need to characterize the right-hand side operator in (6.1), $\mathfrak{L}_0 := \partial/\partial x_2\{\kappa(x_1, x_2)\partial \cdot/\partial x_2\}$ with ℓ_2-periodic boundary conditions, in $\mathbb{H}_{[0,\ell_2]}$.

For example, in the case where the heterogeneity is constant with respect to x_2, a complete set of linearly independent eigenfunctions of $\mathfrak{L}_0$ are $e^{ink_2x_2}$ for every integer n. The spectrum of eigenvalues at (x_0, x_1) is then $\lambda_n(x_1) := -\kappa(x_1)k_2^2 n^2$. This spectrum has one zero-eigenvalue and the rest are negative: $\lambda_n(x_1) \leq -\kappa(x_1)k_2^2 < 0$. Hence, for every x_0, x_1, the nonzero eigenvalues satisfy $\lambda_n(x_1) \leq -\kappa_{\min}k_2^2 < 0$.

For general heterogeneity, similar deductions to those of Section 3.1 establish that the operator $\mathfrak{L}_0$ is self-adjoint. Hence, the eigenvalues are real and eigenfunctions orthogonal. By a similar argument to that of Section 3.1, it follows that the nonzero eigenvalues of the operator are bounded above by $\lambda \leq -\beta_2$ for $\beta_2 := \kappa_{\min} k_2^2 = 4\pi^2 \kappa_{\min}/\ell_2^2$.

Slowly varying theory. We proceed analogously to Section 3.2, but now with two space dimensions (x_0 and x_1) in which solutions are slowly varying. Roberts and Bunder [55] developed rigorous slow manifold theory for spatio-temporal systems that have slow variations in multiple space dimensions. The operator $\mathfrak{L}_0$ satisfies the preconditions in [55, Assumption 3] with one zero eigenvalue ($m = 1, \alpha = 0$) and the rest negative. By [55, Proposition 1], and analogous to Proposition 3.3, we are assured that in a regime of slowly varying solutions, the mesoscale field $\mathfrak{U}(t, x_0, x_1)$ satisfies a PDE akin to (3.2), but in 2D space, to a quantified error [55, (52)], and upon neglecting exponentially decaying transients (decaying faster than $e^{-\beta' t}$ for $\beta' \approx \beta_2$).

A generating function argument [55, Sections 3.2–3.3] establishes the validity of formal 'slowly varying' analysis of the embedding PDE (2.1).

An example mesoscale homogenization. Appendix B lists and documents CAS code to construct the mesoscale homogenization for the example case of heterogeneous diffusivity

$$\kappa(x_1, x_2) := 1/[1/\mathfrak{K}(x_1) + a_2 \cos k_2 x_2] \quad \text{for } k_2 := 2\pi/\ell_2, \tag{6.2}$$

and some given mesoscale heterogeneity function $\mathfrak{K}(x_1)$. The code derives that in terms of the mesoscale mean $\mathfrak{U}(t, x_0, x_1)$, and in terms of $\mathfrak{D}_x := \partial_{x_0} + \partial_{x_1}$, the microscale field (cf. (4.2a)) is

$$\mathfrak{u} = \mathfrak{U} + \frac{\mathfrak{K}(x_1) a_2 \sin k_2 x_2}{k_2} \mathfrak{D}_x \mathfrak{U} + \mathfrak{D}_x \left\{ \frac{\mathfrak{K}(x_1) a_2 \cos k_2 x_2}{k_2^2} \mathfrak{D}_x \mathfrak{U} \right\} + O(\mathfrak{D}_x^3). \tag{6.3}$$

Simultaneously, the code derives that the mesoscale mean field evolves according to the quasi-diffusion PDE

$$\frac{\partial \mathfrak{U}}{\partial t} = \mathfrak{D}_x \{ \mathfrak{K}(x_1) \mathfrak{D}_x \mathfrak{U} \} + \frac{a_2^2}{2k_2^2} \mathfrak{D}_x \{ \mathfrak{K}(x_1)^2 \mathfrak{D}_x^2 [\mathfrak{K}(x_1) \mathfrak{D}_x \mathfrak{U}] \} + O(\mathfrak{D}_x^6). \tag{6.4}$$

As to be expected, the leading-order effective diffusivity on the mesoscale, $\mathfrak{K}(x_1)$, is the harmonic mean over x_2 of the microscale diffusivity (6.2). The theory of this subsection assures us that a truncation of the PDE (6.4) models the dynamics of the embedded PDE (2.1) whenever and wherever the spatial gradients in x_0 and x_1 are 'small' enough on the microscale ℓ_2. That is, PDE (6.4) is a mesoscale model.

6.2. Homogenization of the mesoscale model

The mesoscale PDE (6.4) is heterogeneous on the spatial length scale ℓ_1 of variations in the coefficient $\mathfrak{K}(x_1)$. For the case $\ell_1 \ll L$, we here derive the macroscale homogenization of this mesoscale model.

We have to choose some truncation of PDE (6.4) to analyse further, so let us choose the leading order truncation $\mathfrak{U}_t = \mathfrak{D}_x\{\mathfrak{K}(x_1)\mathfrak{D}_x\mathfrak{U}\}$ as the mesoscale model.

To compare with the one-step homogenization, let us consider PDE (6.4) in the case where the mesoscale diffusivity is

$$\mathfrak{K}(x_1) := 1/[1 + a_1 \cos k_1 x_1] \quad \text{for } k_1 := 2\pi/\ell_1 .$$

The theory and construction of the homogenization follow the same procedure as detailed before, so let us just summarize here. First, we treat derivatives $\partial/\partial x_0$ as 'small'. Then the cross-sectional cell PDE is

$$\frac{\partial \mathfrak{U}}{\partial t} = \frac{\partial}{\partial x_1}\left\{\mathfrak{K}(x_1)\frac{\partial \mathfrak{U}}{\partial x_1}\right\}, \tag{6.5}$$

to be solved with ℓ_1-periodic boundary conditions in x_1, and in space $\mathcal{H}_{[0,\ell_1]}$.

Second, a subspace of equilibria of (6.5) is $\mathfrak{U}(t, x_1) = U$, constant in x_1. The spectrum of the linear operator $\mathcal{L}_0 := \partial/\partial x_1\{\mathfrak{K}(x_1)\partial\cdot/\partial x_1\}$ can be straightforwardly shown to be self-adjoint with one zero eigenvalue, and the rest negative and bounded away from zero, $\lambda \le -\beta_1$, for $\beta_1^2 := k_1^2\mathfrak{K}_{\min} = 4\pi^2\mathfrak{K}_{\min}/\ell_1^2$.

Third, slowly varying theory for cylindrical domains, akin to Section 3.2, applies to assure us there exists a slow manifold homogenization of the mesoscale model in terms of a macroscale mean field $U(t, x_0)$. Further, the slow manifold emerges exponentially quickly on a time scale of $1/\beta_1$, and we may approximate the slow manifold via formal 'slowly varying' analysis of the mesoscale PDE (6.4).

Fourth, the construction from the mesoscale PDE $\mathfrak{U}_t = \mathfrak{D}_x\{\mathfrak{K}(x_1)\mathfrak{D}_x\mathfrak{U}\}$ to the macroscale homogenization is the specific case of Section 4 with $a_2 = 0$ and no variable x_2. Consequently, corresponding results follow immediately, such as the slow manifold is (4.2a) with $a_2 = 0$, and the macroscale homogenization is $U_t = U_{xx}$ to errors $O(\partial_x^4)$.

Here there is no point proceeding to higher order error in ∂_x, because we chose the leading order mesoscale PDE at the start of this subsection. To obtain correct higher-order macroscale homogenizations, we would chose a correspondingly higher-order mesoscale homogenization.

7. Conclusion

This article further develops a novel theory and practice for mathematical/asymptotic homogenization to illuminate and resolve many issues in homogenizing heterogeneous PDEs such as (1.1). Section 2 introduces the technique of analysing an ensemble of all phase shifts, and extends it to multi-periodic cases, including the case of quasi-periodic. Future research may be able to extend the approach to interesting classes of random heterogeneity. The key to this approach is to be able to recast the ensemble as a system which is mathematically homogeneous in the macroscale.

Given the mathematically homogeneous macroscale ensemble, Section 3 applies recent developments of dynamical systems theory to newly establish the homogenization as a rigorous slow manifold of the given PDE system. No "ϵ" is required so the results hold for *finite* scale separation. No variational principles are required, so the approach applies to a wide range of physical problems, both dissipative and wave-like. The dynamical systems approach provides a framework that future research and applications may exploit to rigorously derive accurate initial conditions, boundary conditions, forcing projections, uncertainty evaluation and error bounds.

This dynamical systems framework provides a very practical way to construct homogenized models, as in the example of Section 4, and as in Appendix A. It illustrates the ease in using computer algebra to perform and check the homogenization (4.2). The method systematically and straightforwardly extends to higher order to derive so-called "second-order homogenization": indeed, Appendix A.2 simply proceeds further to explicitly construct the "fourth-order homogenization" (4.3).

One advantage in the computer algebra is that, for some classes of heterogeneities, we can proceed to very high order in the analysis. Section 5 computed to 34th-order and uses the resulting generalized homogenization to quantify how 'much smaller' the microscale really has to be compared with the macroscale. Remarkably, the evidence is that, ideally, macroscale lengths can be resolved down to just twice the microscale length! Of course, in practice, there are many confounding aspects, but this factor of two is the mathematically ideal lower bound.

The spatio-temporal resolution of homogenizations could be improved, in future research, by multi-modal/multi-zonal homogenization of the heterogeneous microscale system by adapting approaches developed for shear dispersion [56, 69]. Such multi-modal/multi-zonal homogenization would be akin to Timoshenko–Ehrenfest beam theory [66, 71].

Lastly, Section 6 explores how the approach developed here includes the case when there are three separated length scales in the physical problem: a microscale, mesoscale and macroscale. The exploration shows how one can analyse such a system in one step from the combined micro and meso scales to the macroscale, or one can analyse the system in two steps from micro to meso, and then from meso to macro. Because sound modelling is transitive, the resulting homogenizations are the same. Further, if one's ultimate aim is a macroscale spatial discretization to compute predictions, that is, the aim is not really the homogenized PDE, then instead of the two-step process of first homogenization and second spatial discretization, future research could do it all in one step from microscale heterogeneous PDE to macroscale discretization using a process like that introduced in a shear dispersion example [37].

A. Appendix: Computer algebra to construct a homogenized PDE

The following code constructs the homogenization (3.2), discussed in Section 4, of the PDEs (1.1) and (2.1) for the family of problems with diffusivity (4.1) for microscale periodicities ℓ_1, ℓ_2. Let us use the computer algebra system REDUCE

(http://www.reduce-algebra.com) as it is free, flexible and fast [27]. First improve the printed output:

```
17    on div; off allfac; on revpri;
18    factor d,df;
```

Let the arguments of trig function heterogeneity be denoted by q_i and define wavenumbers $k_i := 2\pi/\ell_i$, so the diffusivity $\kappa(x_1, x_2)$ is the following.

```
24    depend q1,x1,z; depend q2,x2,z;
25    let { df(q1,x1)⇒k1, df(q2,x2)⇒k2 };
26    kappa:=1/(1+a1*cos(q1)+a2*cos(q2));
```

Write approximations to the slow manifold model of the embedding PDE (2.1) in terms of a "mean" field $U(t, x)$, denoted by uu, that evolves according to $\partial U/\partial t = $ dudt for whatever dudt happens to be.

```
36    depend uu,x,t;
37    let df(uu,t)⇒dudt;
```

This code uses x for x_0 as the two are synonymous in practice.

A.1. Quickly verify a leading approximation   First, we guess and then verify the approximate field (4.2a). This is coded, with ordering parameter d that counts the number of x-derivatives in U, as

```
50    u:=uu+d*(a1/k1*sin(q1)+a2/k2*sin(q2))*df(uu,x)
51        +d^2*(a1/k1^2*cos(q1)+a2/k2^2*cos(q2))*df(uu,x,2);
```

such that U evolves according to the homogenized PDE $\partial U/\partial t = \partial^2 U/\partial x^2 + \cdots$ (the coefficient 1 of the mean diffusivity is the classic harmonic mean of the specific heterogeneous diffusivity (4.1)):

```
58    dudt:=d^2*df(uu,x,2);
```

To verify, substitute into the governing PDE (2.1) and find the PDE's residual is zero to an error $O(\partial_x^3)$—counting the derivatives with the order parameter d.

```
65    let d^3 ⇒ 0;
66    flux:=-kappa*(d*df(u,x)+df(u,x1)+df(u,x2))$
67    pde:=df(u,t)+d*df(flux,x)+df(flux,x1)+df(flux,x2);
```

Since the PDE residual is $O(\partial_x^3)$, then the slow manifold (4.2a) is correct to error $O(\partial_x^3)$ [51].

The next subsection repeatedly computes the residual, to drive corrections, until the residual is zero to a specified order of error, and hence gives a slow manifold to the same order of error.

A.2. Iteration systematically constructs   Second, we iteratively construct the improved homogenization (4.3). This code executes in approximately four seconds.

```
86   write "
87   Second, Iteratively Construct
88   ----------";
```

The terms $O(\partial_x^4)$ appear, at first, impossible to find with exact algebra, so instead we construct in a power series in the amplitude of the heterogeneity. Let `a` count the number of amplitude factors arising from κ. Choose the following order of errors in both derivatives and $a := \sqrt{a_1^2 + a_2^2}$. It eventuates that for this particular heterogeneity κ, the results to error $O(\partial_x^{\mathrm{ord}})$ appear exact in heterogeneity amplitude a.

```
104   ord:=7;
```

Here assume heterogeneity κ is a reciprocal, but could be more general.

```
109   rkappa:=sub(a1=a*a1,a2=a*a2,1/kappa);
```

Optional. We may set $a_2 = 0$ to get simpler results for a single periodic component, and change truncation to the same order, now high-order. Order 35 takes roughly one minute of compute time. The high-order coefficients of the homogenized PDE resulting from this option are exact, as far as they go, because the evidence is that the expansions in homogeneity amplitude a extend to at most the same order as the order of derivatives.

```
121   if 0 then begin a2:=0; a1:=k1:=1; ord:=35; end;
```

In general. Construct heterogeneous diffusivity κ as the reciprocal of `rkappa`, presuming $\kappa \approx 1$:

```
128   kappa:=1+for n:=1:ord-1 sum (1-rkappa)^n$
129   res:=(kappa*rkappa-1 where a^~p =>0 when p>=ord) ;
130   if res neq 0 then rederr("kappa reciprocal error") ;
```

Start the iteration from the trivial approximation for the field and its evolution.

```
137   u:=uu;
138   dudt:=0;
```

Seek solution to the specified orders of errors.

```
142   for it:=1:999 do begin write "
143   **** ITERATION ", it;
```

Progressively truncate the order of the order parameter so that we control the residuals better: the bound in this if-statement is the aimed for ultimate order of error.

```
150    if it<ord then let {d^(it+1)=>0, a^(it+1)=>0};
```

Compute the PDE residual via the flux, trace printing the length of the residual expression:

```
155    flux:=-kappa*(d*df(u,x)+df(u,x1)+df(u,x2));
156    pde:=df(u,t)+d*df(flux,x)+df(flux,x1)+df(flux,x2);
157    pde:=trigsimp(pde,combine);
158    write lengthpde:=length(pde);
```

Update the evolution via the solvability condition from the mean over x_1, x_2:

```
163    gd:=-(pde where {sin(~a)=>0,cos(~a)=>0});
164    if it<6 then write gd:=gd else write lengthgd:=length(gd);
165    dudt:=dudt+gd;
166    rhs:=pde+gd;
```

Attempt to solve the update in two steps, each step with two integrals. Use the following operator, given we already made `qi` depend upon dummy `z`.

```
173    if it=1 then begin
174      operator intx; linear intx;
175      let { intx(cos(~q),z) => sin(q)/(df(q,x1)+df(q,x2))
176          , intx(sin(~q),z) =>-cos(q)/(df(q,x1)+df(q,x2))
177          };
178    end;
```

- First integrate $v_{x_1} + v_{x_2} =$ `rhs` with zero mean. If any `intx(1,z)` appear, then mistake.

  ```
  184    v:=trigsimp( intx(rhs,z));
  185    if not freeof(v,intx(1,z)) then rederr("ABORT");
  ```

- Second, solve $\kappa u'_z = \kappa(u'_{x_1} + u'_{x_2}) = v$, using divide by κ and integrate again. Assume any presence of `intx(1,z)` is an error that eventually sorts itself out in the iteration, so obliterate here! The update then has mean zero.

  ```
  193    ud:=intx(trigsimp(v*rkappa,combine),z);
  194    ud:=(ud where intx(1,z)=>0); % obliterate
  ```

Add in the update. Perhaps trigsimp is useful here.

```
199    u:=u+trigsimp(ud);
```

Exit iterative for-loop when the PDE residual is zero

```
204        if pde=0 then write "Success: ", it:= it+10000;
205    end;
```

```
206   showtime;
207   if pde neq 0 then rederr("Iteration failure");
```

Write out homogenized PDE, optionally its coefficients, and end the script.

```
213   dudt:=dudt;
214   if ord>7 then begin cs:=coeff(dudt,d);
215       cs:=for n:=3 step 2 until length(cs)
216           collect part(cs,n)/df(uu,x,n-1);
217       on rounded; off nat; write cs:=cs;
218       on nat; off rounded; end;
219   end;
```

B. Appendix: Meso-scale homogenization code

Construct the asymptotic expansion of the meso-slow homogenization of three-scale diffusion supported by the theory of Section 6.1.

```
11   on div; off allfac; on revpri;
12   factor d,b,a2,k2;
```

The diffusivity $\kappa(x_1, x_2)$ is the following, where $b(n)$ denotes the nth derivative of $b(x_1)$. At the end, we recast in $c = \Re(x_1) := 1/b(x_1)$.

```
18   depend kappa,x1,x2;
19   operator b; depend b,x1;
20   kappa:=1/(b(0)+a2*cos(k2*x2));
21   let { df(b(~n),x1) => b(n+1) };
```

Write approximations to the slow manifold model of the embedding PDE (2.1) in terms of a "mean" field $U(t, x)$ that evolves according to $\partial U/\partial t = $ dudt.

```
29   depend uu,x,x1,t;
30   let df(uu,t)=>dudt;
```

This code uses x for x_0 as the two are synonymous in practice. Start from the leading approximation for the field and its evolution.

```
36   u:=uu$
37   dudt:=0$
```

Iteratively construct to this order of error in slow derivatives.

```
43   ordd:=5;
44   for it:=1:999 do begin write "
45   **** Iteration ",it;
```

Progressively truncate the order of the order parameter so that we better control the residuals.

```
50    if it<ordd then let d^(it+1)=>0;
```

Compute the PDE residual via the flux, trace printing the length of the residual expression:

```
55    flux:=-kappa*(d*df(u,x)+d*df(u,x1)+df(u,x2));
56    pde:=df(u,t)+d*df(flux,x)+d*df(flux,x1)+df(flux,x2);
57    pde:=trigsimp(pde);
58    write lengthpde:=length(pde);
```

Solvability updates the evolution:

```
63    dudt:=dudt+(gd:=-int(pde,x2,0,2*pi/k2)/(2*pi/k2));
```

Update the field via some integrals:

```
67    ud:=trigsimp(int(int(pde+gd,x2)/kappa,x2));
68    udx:=sub(x2=2*pi/k2,ud)-sub(x2=0,ud);
69    u:=u+ud-int(ud,x2,0,2*pi/k2)/(2*pi/k2)
70            -udx*(x2-pi/k2+a2/k2/b(0)*sin(k2*x2))/(2*pi/k2);
```

Exit iterative for-loop when the residual is zero.

```
75      showtime;
76      if pde=0 then write "Success: ", it:=it+10000;
77    end;
78    if pde neq 0 then rederr("Iteration failure");
```

Write out homogenized PDE.

```
83    dudt:=dudt;
```

Recast in terms of $c = \Re(x_1) := 1/b(x_1)$.

```
88    operator c; depend c,x1; factor c;
89    let { df(c(~n),x1)=>c(n+1), b(~n)=>df(1/c(0),x1,n) };
90    dudt:=dudt;
```

Check compact form of the evolution PDE and finish the script.

```
94    procedure dx(a); d*(df(a,x)+df(a,x1))$
95    err:=-(dudt where d^5=>0) +dx(c(0)*dx(uu))
96        +a2^2/k2^2/2*dx(c(0)^2*dx(dx(c(0)*dx(uu))));
97    if err neq 0 then rederr("simplification failure");
98    end;
```

Acknowledgements

References

[1]   A. Abdulle and T. Pouchon, "Effective models and numerical homogenization for wave propagation in heterogeneous media on arbitrary timescales", *Found. Comput. Math.* **20** (2020) 1505–1547; doi:10.1007/s10208-020-09456-x.

[2]   G. Allaire, "Homogenization and two-scale convergence", *SIAM J. Math. Anal.* **23** (1992) 1482–1518; doi:10.1137/0523084.

[3]   G. Allaire, A. Lamacz-Keymling and J. Rauch, "Crime pays; homogenized wave equations for long times", *Asymptot. Anal.* **128** (2022) 295–336; doi:10.3233/ASY-211707.

[4]   R. Altmann, P. Henning and D. Peterseim, "Numerical homogenization beyond scale separation", *Acta Numer.* **30** (2021) 1–86; doi:10.1017/S0962492921000015.

[5]   A. Anthoine, "Second-order homogenisation of functionally graded materials", *Int. J. Solids Struct.* **47** (2010) 1477–1489; doi:10.1016/j.ijsolstr.2010.02.004.

[6]   E. Barchiesi, S. R. Eugster, F. Dell'Isola and F. Hild, "Large in-plane elastic deformations of bi-pantographic fabrics: asymptotic homogenization and experimental validation", *Math. Mech. Solids* **25** (2020) 739–767; doi:10.1177/1081286519891228.

[7]   T. B. Benjamin, J. L. Bona and J. J. Mahony, "Model equations for long waves in nonlinear dispersive systems", *Philos. Trans. Roy. Soc. A* **272** (1972) 47–78; doi:10.1098/rsta.1972.0032.

[8]   D. A. Birch and W. R. Young, "A master equation for a spatial population model with pair interactions". *Theor. Popul. Biol.* **70** (2006) 26–42; doi:10.1016/j.tpb.2005.11.007.

[9]   X. Blanc and C. Le Bris, "Improving on computation of homogenized coefficients in the periodic and quasi-periodic settings", *Netw. Heterog. Media* **5** (2010) 1–29; doi:10.3934/nhm.2010.5.1.

[10]   M. P. Brenner and P. Koumoutsakos, "Editorial: Machine learning and physical review fluids: an editorial perspective", *Phys. Rev. Fluids* **6** (2021) Article ID: 070001; doi:10.1103/PhysRevFluids.6.070001.

[11]   D. L. Brown, P. Popov and Y. Efendiev, "On homogenization of Stokes flow in slowly varying media with applications to fluid–structure interaction", *GEM Int. J. Geomath.* **2** (2011) 281–305; doi:10.1007/s13137-011-0025-y.

[12]   J. E. Bunder and A. J. Roberts, "Nonlinear emergent macroscale PDEs, with error bound, for nonlinear microscale systems", *Springer Nat. Appl. Sci.* **3** (2021) 1–28; doi:10.1007/s42452-021-04229-9.

[13]   J. Carr, *Applications of centre manifold theory*, Volume 35 of *Appl. Math. Sci.* (Springer–Verlag, New York, 1981); doi:10.1007/978-1-4612-5929-9.

[14]   C. Chen, A. J. Roberts and J. E. Bunder, "The macroscale boundary conditions for diffusion in a material with microscale varying diffusivities", in: *Proc. 11th Biennial Engineering Mathematics and Applications Conference (EMAC-2013), July 2014* (eds. M. Nelson, T. Hamilton, M. Jennings and J. Bunder) (Queensland University of Technology, Brisbane, Australia, 2014) C218–C234; doi:10.21914/anziamj.v55i0.7853.

[15]   C. Chen, A. J. Roberts and J. E. Bunder, "Macroscale boundary conditions for a non-linear heat exchanger", in: *Proc. 17th Biennial Computational Techniques and Applications Conference (CTAC-2014), December 2014* (eds. J. Sharples and J. Bunder) (Australian National University, Canberra, Australia, 2015) C16–C31; doi:10.21914/anziamj.v56i0.9528.

[16]   C. Chen, A. J. Roberts and J. E. Bunder, "Boundary conditions for macroscale waves in an elastic system with microscale heterogeneity", *IMA J. Appl. Math.* **83** (2018) 1–33; doi:10.1093/imamat/hxy004.

[17] S. Cooper, "Quasi-periodic two-scale homogenisation and effective spatial dispersion in high-contrast media", *Calc. Var. Partial Differential Equations* **57** (2018) 1–33; doi:10.1007/s00526-018-1365-3.

[18] R. Cornaggia and B. B. Guzina, "Second-order homogenization of boundary and transmission conditions for one-dimensional waves in periodic media", *Int. J. Solids Struct.* **188** (2020) 88–102; doi:10.1016/j.ijsolstr.2019.09.009.

[19] S. M. Cox and A. J. Roberts, "Initial conditions for models of dynamical systems", *Phys. D* **85** (1995) 126–141; doi:10.1016/0167-2789(94)00201-Z.

[20] R. V. Craster, "Dynamic Homogenization", in: *Analytic methods in interdisciplinary applications*, Volume 116 of *Springer Proc. Math. Stat.* (eds. V. V. Mityushev and M. Ruzhansky) (Springer, Switzerland, 2015) 41–50; doi:10.1007/978-3-319-12148-2.

[21] O. L. Cruz-González, A. Ramirez-Torres, R. Rodriguez-Ramos, R. Penta and F. Lebon, "Hierarchical heterogeneous one-dimensional problem in linear viscoelastic media", *Eur. J. Mech. A Solids* **95** (2022) Article ID: 104617; doi:10.1016/j.euromechsol.2022.104617.

[22] C. Domb and M. F. Sykes, "On the susceptibility of a ferromagnetic above the Curie point", *Proc. Roy. Soc. Lond. A* **240** (1957) 214–228; doi:10.1098/rspa.1957.0078.

[23] W. J. Drugan and J. R. Willis, "A micromechanics-based nonlocal constitutive equation and estimates of representative volume element size for elastic composites", *J. Mech. Phys. Solids* **44** (1996) 497–524; doi:10.1016/0022-5096(96)00007-5.

[24] M. Duerinckx and A. Gloria, "On the lower spectrum of heterogeneous acoustic operators", Preprint, 2023, arXiv:2304.14046.

[25] M. Duerinckx, A. Gloria and C. Shirley, "Approximate normal forms via Floquet–Bloch theory: Nehorosev stability for linear waves in quasiperiodic media", *Comm. Math. Phys.* **383** (2021) 633–683; doi:10.1007/s00220-021-03966-7.

[26] B. Engquist and P. E. Souganidis, "Asymptotic and numerical homogenization", *Acta Numer.* **17** (2008) 147–190; doi:10.1017/S0962492906360011.

[27] R. Fateman, "Comparing the speed of programs for sparse polynomial multiplication", *ACM SIGSAM Bull.* **37** (2003) 4–15; doi:10.1145/844076.844080.

[28] M. Frank, D. Drikakis and V. Charissis, "Machine-learning methods for computational science and engineering", *Computation* **8** (2020) 1–35; doi:10.3390/computation8010015.

[29] R. González-Garcia, R. Rico-Martinez and I. G. Kevrekidis, "Identification of distributed parameter systems: a neural net based approach", *Comput. Chem. Engrg.* **22** (1998) S965–S968; doi:10.1016/S0098-1354(98)00191-4.

[30] B. Gustafsson and J. Mossino, "Non-periodic explicit homogenization and reduction of dimension: the linear case," *IMA J. Appl. Math.* **68** (2003) 269–298; doi:10.1093/imamat/68.3.269.

[31] A. K. W. Hii and B. El Said, "A kinematically consistent second-order computational homogenisation framework for thick shell models", *Comput. Methods Appl. Mech. Engrg.* **398** (2022) Article ID: 115136; doi:10.1016/j.cma.2022.115136.

[32] P. Hochs and A. J. Roberts, "Normal forms and invariant manifolds for nonlinear, non-autonomous PDEs, viewed as ODEs in infinite dimensions", *J. Differential Equations* **267** (2019) 7263–7312; doi:10.1016/j.jde.2019.07.021.

[33] V. V. Jikov, S. M. Kozlov and O. A. Oleinik, *Homogenization of differential operators and integral functionals* (ed. G. A. Yosifian) (Springer, Berlin–Heidelberg, 1994); doi:10.1007/978-3-642-84659-5.

[34] S. Klarmann, F. Gruttmann and S. Klinkel, "Homogenization assumptions for coupled multiscale analysis of structural elements: beam kinematics", *Comput. Mech.* **65** (2020) 635–661; doi:10.1007/s00466-019-01787-z.

[35] A. J. Linot and M. D. Graham, "Deep learning to discover and predict dynamics on an inertial manifold", *Phys. Rev. E* **101** (2020) Article ID: 062209; doi:10.1103/PhysRevE.101.062209.

[36] E. N. Lorenz and V. Krishnamurthy, "On the non-existence of a slow manifold", *J. Atmos. Sci.* **44** (1987) 2940–2950; doi:10.1175/1520-0469(1987)044<2940:OTNOAS>2.0.CO;2.

[37] T. MacKenzie and A. J. Roberts, "Holistic discretisation of shear dispersion in a two-dimensional channel", in: *Proc. of 10th Computational Techniques and Applications Conference CTAC-2001*, Volume 44 (eds. K. Burrage and R. B. Sidje) (CTAC, 2003) C512–C530; doi:10.21914/anziamj.v44i0.694.

[38] K. Matous, M. G. D. Geers, V. G. Kouznetsova and A. Gillman, "A review of predictive nonlinear theories for multiscale modeling of heterogeneous materials", *J. Comput. Phys.* **330** (2017) 192–220; doi:10.1016/j.jcp.2016.10.070.

[39] B. S. Mercer, K. K. Mandadapu and P. Papadopoulos, "Novel formulations of microscopic boundary-value problems in continuous multiscale finite element methods", *Comput. Methods Appl. Mech. Engrg.* **286** (2015) 268–292; doi:10.1016/j.cma.2014.12.021.

[40] G. N. Mercer and A. J. Roberts, "A centre manifold description of contaminant dispersion in channels with varying flow properties", *SIAM J. Appl. Math.* **50** (1990) 1547–1565; doi:10.1137/0150091.

[41] G. N. Mercer and A. J. Roberts, "A complete model of shear dispersion in pipes", *Jpn. J. Ind. Appl. Math.* **11** (1994) 499–521; doi:10.1007/BF03167234.

[42] R. G. Muncaster, "Invariant manifolds in mechanics I: the general construction of coarse theories from fine theories", *Arch. Ration. Mech. Anal.* **84** (1984) 353–373; doi:10.1007/BF00250587.

[43] V. P. Nguyen, M. Stroeven and L. J. Sluys, "Multiscale continuous and discontinuous modeling of heterogeneous materials: a review on recent developments", *J. Multiscale Model.* **3** (2011) 229–270; doi:10.1142/S1756973711000509.

[44] I. Niyonzima, "Multiscale Finite Element Modeling of Nonlinear Quasistatic Electromagnetic Problems", Ph.D. Thesis, Université de Liège, Faculté des Sciences Appliquées, 2014.

[45] A. Ramirez-Torres, R. Penta, R. Rodriguez-Ramos, J. Merodio, F. J. Sabina, J. Bravo-Castillero, R. Guinovart-Diaz, L. Preziosi and A. Grillo, "Three scales asymptotic homogenization and its application to layered hierarchical hard tissues", *Int. J. Solids Struct.* **130–131** (2018) 190–198; doi:10.1016/j.ijsolstr.2017.09.035.

[46] A. J. Roberts, "The application of centre manifold theory to the evolution of systems which vary slowly in space", *J. Aust. Math. Soc. B* **29** (1988) 480–500 (now *ANZIAM J.*); doi:10.1017/S0334270000005968.

[47] A. J. Roberts, "Appropriate initial conditions for asymptotic descriptions of the long term evolution of dynamical systems", *J. Aust. Math. Soc. B* **31** (1989) 48–75 (now *ANZIAM J.*); doi:10.1017/S0334270000006470.

[48] A. J. Roberts, "Boundary conditions for approximate differential equations", *J. Aust. Math. Soc. B* **34** (1992) 54–80 (now *ANZIAM J.*); doi:10.1017/S0334270000007384.

[49] A. J. Roberts, "The invariant manifold of beam deformations. Part 1: the simple circular rod", *J. Elasticity* **30** (1993) 1–54; doi:10.1007/BF00041769.

[50] A. J. Roberts, "Low-dimensional modelling of dynamics via computer algebra", *Computer Phys. Comm.* **100** (1997) 215–230; doi:10.1016/S0010-4655(96)00162-2.

[51] A. J. Roberts, "Computer algebra derives correct initial conditions for low-dimensional dynamical models", *Computer Phys. Comm.* **126** (2000) 187–206; doi:10.1016/S0010-4655(99)00494-4.

[52] A. J. Roberts, "Macroscale, slowly varying, models emerge from the microscale dynamics in long thin domains", *IMA J. Appl. Math.* **80** (2015) 1492–1518; doi:10.1093/imamat/hxv004.

[53] A. J. Roberts, *Model emergent dynamics in complex systems* (SIAM, Philadelphia, PA, 2015); doi:10.1137/1.9781611973563.

[54] A. J. Roberts, "Backwards theory supports modelling via invariant manifolds for non-autonomous dynamical systems", Preprint, 2022, arXiv:1804.06998.

[55] A. J. Roberts and J. E. Bunder, "Slowly varying, macroscale models emerge from microscale dynamics over multiscale domains", *IMA J. Appl. Math.* **82** (2017) 971–1012; doi: 10.1093/imamat/hxx021.

[56] A. J. Roberts and D. V. Strunin, "Two-zone model of shear dispersion in a channel using centre manifolds", *Quart. J. Mech. Appl. Math.* **57** (2004) 363–378; doi:10.1093/qjmam/57.3.363.

[57] I. A. Rodrigues Lopes and F. M. Andrade Pires, "Unlocking the potential of second-order computational homogenisation: an overview of distinct formulations and a guide for their implementation", *Arch. Comput. Methods Eng.* **29** (2022) 1339–1393; doi:10.1007/s11831-021-09611-9.

[58] P. Romanazzi, M. Bruna and D. Howey, "Thermal homogenisation of electrical machine windings applying the multiple-scales method", *J. Heat Transf.* **139** (2016) Article ID: 012101; doi:10.1115/1.4034337.

[59] S. Saeb, P. Steinmann and A. Javili, "Aspects of computational homogenization at finite deformations: a unifying review from Reuss' to Voigt's bound", *Appl. Mech. Rev.* **68**(5) (2016) Article ID: 050801; doi:10.1115/1.4034024.

[60] M. Schneider, "A review of nonlinear FFT-based computational homogenization methods", *Acta Mech.* **232** (2021) 2051–2100; doi:10.1007/s00707-021-02962-1.

[61] D. P. Shahraki and B. B. Guzina, "Homogenization of the wave equation with non-uniformly oscillating coefficients", *Math. Mech. Solids* **27**(11) (2022) 2341–2365; doi:10.1177/10812865211065098.

[62] J. Somnic and B. W. Jo, "Homogenization methods of lattice materials", *Encyclopedia* **2** (2022) 1091–1102; doi:10.3390/encyclopedia2020072.

[63] J. Somnic and B. W. Jo, "Status and challenges in homogenization methods for lattice materials", *Materials* **15** (2022) Article ID: 605; doi:10.3390/ma15020605.

[64] S. H. Strogatz, *Nonlinear dynamics and chaos: with applications to physics, biology, chemistry, and engineering*, (*Studies in Nonlinearity*) (Addison-Wesley, Boca Raton, FL, 1994); doi:10.1201/9780429492563.

[65] G. Teschl, *Ordinary differential equations and dynamical systems*, Volume 140 of *Grad. Stud. Math.* (American Mathematical Society, Providence, RI, 2012); http://www.mat.univie.ac.at/~gerald/ftp/book-ode/.

[66] S. P. Timoshenko and S. Woinowsky-Krieger, *Theory of shells and plates* (McGraw Hill, New York, 1959), https://archive.org/details/TheoryOfPlatesAndShells.

[67] M. van Dyke, "Computer-extended Series", *Annu. Rev. Fluid Mech.* **16** (1984) 287–310; doi:10.1146/annurev.fl.16.010184.001443.

[68] N. G. van Kampen, *Stochastic processes in physics and chemistry* (Elsevier, Amsterdam, Netherlands, 1992); doi:10.1016/B978-0-444-52965-7.50023-4.

[69] S. D. Watt and A. J. Roberts, "The accurate dynamic modelling of contaminant dispersion in channels", *SIAM J. Appl. Math.* **55** (1995) 1016–1038; doi:10.1137/S0036139993257971.

[70] Z. Welsh, M. J. Simpson, Md I. H. Khan and M. A. Karim, "Multiscale modeling for food drying: state of the art", *Compr. Rev. Food Sci. Food Saf.* **17** (2018) 1293–1308; doi:10.1111/1541-4337.12380.

[71] Wikipedia, Timoshenko–Ehrenfest beam theory (2022). https://en.wikipedia.org/wiki/TimoshenkoE28093Ehrenfest_beam_theory.